REPORT NO.
UCD/CGM-01/03

CENTER FOR GEOTECHNICAL MODELING

FINITE DEFORMATION ANALYSIS OF GEOMATERIALS

BY

B. JEREMIC
K. RUNESSON
S. STURE

DEPARTMENT OF CIVIL & ENVIRONMENTAL ENGINEERING
COLLEGE OF ENGINEERING
UNIVERSITY OF CALIFORNIA AT DAVIS

SEPTEMBER 2001

University of Califorina at Davis, Center for Geotechnical Modeling Report UCD-CGM-01
Published in the International Journal for Numerical and Analytical Methods in Geomechanics incorporating Mechanics of Cohesive–Frictional Materials, Vol. 25, No. 8, pp. 809-840, 2001.

Finite Deformation Analysis of Geomaterials

B. Jeremić [1] **K. Runesson** [2] **S. Sture** [3]

[1]Department of Civil and Environmental Engineering, University of California, Davis 95616, U.S.A. phone 530.754.9248, fax 530.752.7872, Email: `Jeremic@UCDavis.edu`.

[2]Division of Solid Mechanics, Chalmers University of Technology, S-41296 Göteborg, Sweden

[3]Department of Civil, Environmental, and Architectural Engineering, University of Colorado, Boulder, CO 80309-0428, U.S.A.

Abstract

The mathematical structure and numerical analysis of classical small deformation elasto–plasticity is generally well established. However, development of large deformation elastic–plastic numerical formulation for dilatant, pressure sensitive material models is still a research area.

In this paper we present development of the finite element formulation and implementation for large deformation, elastic–plastic analysis of geomaterials. Our developments are based on the multiplicative decomposition of the deformation gradient into elastic and plastic parts. A consistent linearization of the right deformation tensor together with the Newton method at the constitutive and global levels leads toward an efficient and robust numerical algorithm. The presented numerical formulation is capable of accurately modeling dilatant, pressure sensitive *isotropic* and *anisotropic* geomaterials subjected to large deformations. In particular, the formulation is capable of simulating the behavior of geomaterials in which eigentriads of stress and strain do not coincide during the loading process.

The algorithm is tested in conjunction with the novel hyperelasto–plastic model termed the **B** material model, which is a single surface (single yield surface, affine single ultimate surface and affine single potential surface) model for dilatant, pressure sensitive, hardening and softening geomaterials. It is specifically developed to model large deformation hyperelasto–plastic problems in geomechanics.

We present an application of this formulation to numerical analysis of low confinement tests on cohesionless granular soil specimens recently performed in a SPACEHAB module aboard the Space Shuttle during the STS-89 mission. We compare numerical modeling with test results and show the significance of added confinement by the thin hyperelastic latex membrane undergoing large stretching.

Key Words: Hyperelasto–plasticity, Large deformations, Geomaterials, Finite element analysis

1 Background

Theoretical as well as implementation issues in material non–linear finite element analysis of solids and structures are increasingly becoming better understood for the case of infinitesimal strain theories. Likewise, large deformation theories and implementations for materials obeying J_2 plasticity rules are fairly advanced. Large strain analysis involving geometric and material non–linearities or pressure sensitive geomaterials are still the subject of active research. The choice of appropriate stress and strain measures, as well as the issues pertaining to the integration of elasto–plastic constitutive equations under conditions of large strain are still disputed in the research community.

The key assumption in infinitesimal deformation elasto–plasticity is the additive decomposition of strains into elastic and plastic parts. A number of generalized mid–point numerical algorithms, ranging from purely explicit to purely implicit schemes was developed and their accuracy assessed (Crisfield [9], Kojić and Bathe [20], Ortiz and Popov [35], Simo and Taylor [48], Ortiz and Simo [36], Runesson et. al. [41], Krieg and Krieg [22] to mention a few). Implicit, backward Euler integration schemes have in recent years been proven to be robust and efficient. Algorithmic tangent stiffness tensors have been derived (starting with the pioneering work of Simo and Taylor [48] and Runesson and Samuelsson [40]) for most of the integration schemes.

It is important to note that strains are non–linear functions of displacements and thus additive decomposition of total strains into elastic and plastic components hold only for infinitesimal deformations (see more in Lubarda and Lee [29] and Famiglietti and Prevost [13]) Moreover, a simple example is presented, which illustrates differences between large and small deformation analysis. The response of a solid in terms of small and large deformations is compared. To this end we use the definition of a deformation gradient $F_{ij} = x_{i,j}$ and the Lagrangian strain tensor E_{ij}) and compare it with the small deformation strain tensor ϵ_{ij}. Clearly the difference between E_{ij} and ϵ_{ij} is in the nonlinear term of displacement derivatives:

$$E_{ij} = \frac{1}{2}\left(u_{i,j} + u_{j,i} + u_{i,j}u_{j,i}\right) \qquad \epsilon_{ij} = \frac{1}{2}(u_{i,j} + u_{j,i}) \tag{1}$$

Only very small deformations can approximate E_{ij} with ϵ_{ij}. The error exceeds 10% after a nominal strain of 30%. Fig. 1 shows that by using the small deformation strain measure instead of the large deformation strain, significant error is introduced.

The early extensions to large deformation of rate based numerical methods for elasto–

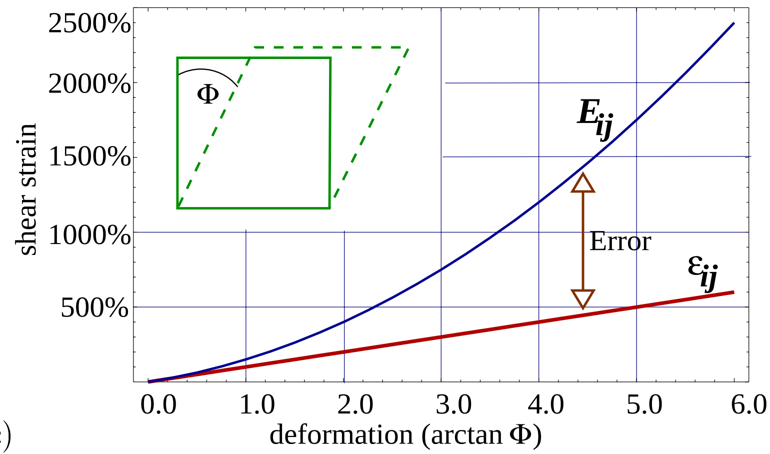

c)

Figure 1: Error introduced by using the small strain instead of Lagrangian strain tensor.

plastic analysis of solids was conducted in the Lagrangian form[1]. Large deformation principle of virtual work based formulation for large strain elastic–plastic analysis of solids in the Lagrangian form was proposed by Hibbitt et al. [16]. The Eulerian form of the solution to the problem was proposed by McMeeking and Rice [32]. The disadvantage with this approach was in the necessary use of incrementally objective integration algorithms that may be computationally expensive. Hypoelastic based techniques, aimed at problems with small elastic strains were also proposed by many others, (see for example Saran and Runesson [42]). A number of problems encountered with different stress rates were noted by Nagtegaal and de Jong [34], Kojić and Bathe [21] and Szabó and Balla [52].

On the other hand, hyperelastic based techniques have been developed recently for purely deviatoric plasticity, for example by Simo and Ortiz [47], [45], Bathe et al. [2], Simo [43], [44], Eterovic and Bathe [12], Perić et al. [39] and Cuitino and Ortiz [10]. Most of the multiplicative split techniques are based on the earlier works of Hill [17], Bilby et al. [3] Kröner [23], Lee and Liu [26], Fox [14] and Lee [25].

Simo and Ortiz [47] where the first to propose a computational approach entirely based on the multiplicative decomposition of the deformation gradient. Their stress update algorithm, however, used the cutting plane scheme that has been shown by de Borst and Feenstra [11] to yield erroneous results for some yield criteria. Bathe et al. [2] have used the multiplicative decomposition with logarithmic stored energy function and an exponential approximation of the flow rule for non–linear analysis of metals. Eterovic and Bathe [12] included kinematic

[1] Hypoelasticity is presented in spatial format. Virtual work is normally stated in the material format.

hardening in their development, but they did not address the issue of tangent stiffness tensors consistent with the use of the Newton scheme for the solution of finite element equations in the finite deformation regime. They have also explored the use of a series expansion of the Hencky strain tensor in their numerical algorithm. However, developments were made for deviatoric plasticity only.

Perić at al. [39] followed their work and experimented with various rate forms and their approximations. They also restricted the use of their algorithm to the small elastic strain case. Cuitino and Ortiz [10] proposed a method for extending small strain state update algorithms and their corresponding consistent tangent stiffness moduli into the finite deformation regime but, although they claim that the method is applicable to various material models, they stayed with the J_2 plasticity model. Simo [43], [44], explored a strain–space formulation. The analysis was conducted for a linear hardening J_2 plasticity problem. In his later work, Simo [45] consolidated the theoretical framework and showed some excellent examples of three dimensional large deformation J_2 elasto–plastic analysis. Limited application of that work to geomaterials has been shown by Simo and Meschke [46]. They applied the developed framework to the Cam–Clay and general plasticity type of models, used in geotechnics. They have also explored different implicit–explicit schemes for integration of the hardening law in order to bypass the hardening induced non–symmetric tangent stiffness moduli. The shortcoming of that work was that an associated flow rule was adopted, thus resulting in overestimation of dilatation. Moreover, loss of collinearity between stress and strain eigentriads (occurring during non–proportional loading of geomaterials) cannot be modeled with this category of algorithm.

More recently Lewis and Khoei [27] used a rate–based total Langrangean formulation to the analysis of compacted powders. Perić and de Souza Neto [38] used an operator split algorithm in terms of principal stresses in conjunction with the Tresca model. Armero [1] extended the multiplicative algorithm (originally developed by Simo) for a coupled poro–plastic fully saturated medium. Borja and Alarcón [5] [8] used multiplicative decomposition in principal coordinates (Simo's formulation) for the problem of large deformation consolidation. Borja et al. [6], [4], [7] applied Simo's approach to the Cam–Clay family of models. Liu et al. [28] have applied an earlier algorithm developed by Simo [46] and added a new nonlinear elastic law for the analysis of tire–sand composite material. The above developments make an implicit assumption on co–linearity of principal directions of stress and strain tensors, which renders them unusable for anisotropic hardening/softening material models.

In the following, finite element and constitutive formulations for a general hyperelastic–plastic geomaterial are presented. More specifically, section 2 presents a large deformation finite element formulation with focus on the Lagrangian description. Section 3 provides hyperelastic and hyperelastic–plastic background descriptions and describes the constitutive integration algorithm. Selected results are presented in section 4.

2 Material and Geometric Non–Linear Finite Element Formulation

In the following we present a detailed formulation of a material and geometric non–linear static finite element analysis scheme. The configuration of choice is material or Lagrangian. The local form of equilibrium equations in Lagrangian format for the static case can be written as:

$$P_{ij,j} - \rho_0 b_i = 0 \tag{2}$$

where $P_{ij} = S_{kj}(F_{ik})^t$ and S_{kj} are first and second Piola–Kirchhoff stress tensors, respectively and b_i are body forces. The weak form of the equilibrium equations is obtained by premultiplying (2) with virtual displacements δu_i and integrating by parts with reference to the initial configuration B_0 (initial volume V_0):

$$\int_{V_0} \delta u_{i,j} P_{ij} dV = \int_{V_0} \rho_0 \delta u_i b_i dV - \int_{S_0} \delta u_i \bar{t}_i dS \tag{3}$$

It proves beneficial to rewrite the left hand side of (3) by using the symmetric second Piola–Kirchhoff stress tensor S_{ij}:

$$\int_{V_0} \delta u_{i,j} F_{jl} S_{il} dV = \int_{V_0} \frac{1}{2} \left((\delta u_{i,l} + \delta u_{l,i}) + (\delta u_{i,j} u_{j,l} + u_{l,j} \delta u_{j,i}) \right) S_{il} dV \tag{4}$$

where we have used the symmetry of S_{il} and definition for deformation gradient $F_{ki} = \delta_{ki} + u_{k,i}$. With a convenient definition of the differential operator $\hat{E}_{il}({}^1u_i, {}^2u_i)$

$$\hat{E}_{il}({}^1u_i, {}^2u_i) = \frac{1}{2} \left({}^1u_{i,l} + {}^1u_{l,i} \right) + \frac{1}{2} \left({}^1u_{l,j} \, {}^2u_{j,i} + {}^2u_{i,j} \, {}^1u_{j.l} \right) \tag{5}$$

the virtual work equation (4) can be written as:

$$W^{int}(\delta u_i, u_i^{(k)}) + W^{ext}(\delta u_i) = 0 \tag{6}$$

with:

$$W^{int}(\delta u_i, {}^{n+1}_{\ 0}u_i^{(k)}) \ = \ \int_{\Omega_c} \hat{E}_{ij}(\delta u_i, {}^{n+1}_{\ 0}u_i^{(k)})\ {}^{n+1}_{\ 0}S_{ij}^{(k)}\ dV \tag{7}$$

$$W^{ext}(\delta u_i) \ = \ -\int_{\Omega_c} \rho_0\ \delta u_i\ {}^{n+1}_{\ 0}b_i\ dV - \int_{\partial\Omega_c} \delta u_i\ {}^{n+1}_{\ 0}t_i\ dS \tag{8}$$

We choose a Newton type procedure for satisfying equilibrium. Given the displacement field $u_i^{(k)}(X_j)$, in iteration k, the iterative change $\Delta u_i = u_i^{(k+1)} - u_i^{(k)}$ is obtained from the linearized virtual work expression

$$W(\delta u_i, u_i^{(k+1)}) \simeq W(\delta u_i, u_i^{(k)}) + \Delta W(\delta u_i, \Delta u_i; u_i^{(k)}) \tag{9}$$

Here, $W(\delta u_i, u_i^{(k)})$ is the virtual work expression

$$W(\delta u_i, u_i^{(k)}) = W^{int}(\delta u_i, u_i^{(k)}) + W^{ext}(\delta u_i) \tag{10}$$

where $\Delta W(\delta u_i, \Delta u_i; u_i^{(k)})$ is the linearization of virtual work

$$\begin{aligned}\Delta W(\delta u_i, \Delta u_i; u_i^{(k)}) \ &= \ \lim_{\epsilon\to 0} \frac{\partial W(\delta u_i, u_i + \epsilon\Delta u_i)}{\partial\epsilon} \\ &= \ \int_{\Omega_c} \hat{E}_{ij}(\delta u_i, u_i)\ \mathcal{L}_{ijkl}\ \hat{E}_{kl}(\Delta u_i, u_i)\ dV + \int_{\Omega_c} \Delta\hat{E}_{ij}(\delta u_i, u_i)\ S_{ij}\ dV\end{aligned} \tag{11}$$

Here we have used $dS_{ij} = 1/2\ \mathcal{L}_{ijkl} dC_{kl} = \mathcal{L}_{ijkl}\hat{E}_{kl}(\Delta u_i, u_i)$.

In order to obtain expressions for the stiffness matrix we shall elaborate further on (11). To this end, (11) can be rewritten by expanding the definition for $\hat{E}$ as

$$\begin{aligned}\Delta W(\delta u_i, \Delta u_i; u_i^{(k)}) \ = \ & \\ & \frac{1}{4}\int_{\Omega_c} ((\delta u_{j,i} + \delta u_{i,j}) + (u_{j,r}\delta u_{r,i} + \delta u_{i,r}u_{r,j})) \\ & \mathcal{L}_{ijkl}\,((\Delta u_{k,l} + \Delta u_{l,k}) + (u_{k,s}\Delta u_{s,l} + \Delta u_{l,s}u_{s,k}))\ dV + \\ & + \int_{\Omega_c} \frac{1}{2}\,(\Delta u_{j,l}\delta u_{l,i} + \delta u_{i,l}\Delta u_{l,j})\, S_{ij}\ dV\end{aligned} \tag{12}$$

Or, by conveniently splitting the above equation we can write

$$\begin{aligned}\Delta^1 W(\delta u_i, \Delta u_i; u_i^{(k)}) \ = \ & \\ & \frac{1}{4}\int_{\Omega_c} ((\delta u_{j,i} + \delta u_{i,j}) + (u_{j,r}\delta u_{r,i} + \delta u_{i,r}u_{r,j})) \\ & \mathcal{L}_{ijkl}\ ((\Delta u_{k,l} + \Delta u_{l,k}) + (u_{k,s}\Delta u_{s,l} + \Delta u_{l,s}u_{s,k}))\ dV\end{aligned} \tag{13}$$

$$\Delta^2 W(\delta u_i, \Delta u_i; u_i^{(k)}) = \int_{\Omega_c} \frac{1}{2} \left(\Delta u_{j,l} \delta u_{l,i} + \delta u_{i,l} \Delta u_{l,j} \right) S_{ij} \, dV \tag{14}$$

By further reorganizing (13) and collecting terms we can write:

$$\begin{aligned} \Delta^1 W(\delta u_i, \Delta u_i; u_i^{(k)}) = & \int_{\Omega_c} \left(\frac{1}{2} (\delta u_{j,i} + \delta u_{i,j}) \right) \mathcal{L}_{ijkl} \left(\frac{1}{2} (\Delta u_{k,l} + \Delta u_{l,k}) \right) dV \\ + & \int_{\Omega_c} \left(\frac{1}{2} (\delta u_{j,i} + \delta u_{i,j}) \right) \mathcal{L}_{ijkl} \left(\frac{1}{2} (u_{k,s} \Delta u_{s,l} + \Delta u_{l,s} u_{s,k}) \right) dV \\ + & \int_{\Omega_c} \frac{1}{2} (u_{j,r} \delta u_{r,i} + \delta u_{i,r} u_{r,j}) \mathcal{L}_{ijkl} \frac{1}{2} (u_{k,s} \Delta u_{s,l} + \Delta u_{l,s} u_{s,k}) \, dV \\ + & \int_{\Omega_c} \frac{1}{2} (u_{j,r} \delta u_{r,i} + \delta u_{i,r} u_{r,j}) \mathcal{L}_{ijkl} \left(\frac{1}{2} (\Delta u_{k,l} + \Delta u_{l,k}) \right) dV \end{aligned} \tag{15}$$

It should be noted that the Algorithmic Tangent Stiffness (ATS) tensor $\mathcal{L}_{ijkl}$ possesses both minor symmetries ($\mathcal{L}_{ijkl} = \mathcal{L}_{jikl} = \mathcal{L}_{ijlk}$). However, major symmetry cannot be guaranteed. Non–associated flow rules in elastoplasticity lead to the loss of major symmetry ($\mathcal{L}_{ijkl} \neq \mathcal{L}_{klij}$). Moreover, it can be shown (i.e. [19]) that an algorithmically induced symmetry loss is observed even for associated flow rules.

Upon observing minor symmetry of $\mathcal{L}_{ijkl}$ one can write (15) as:

$$\begin{aligned} \Delta^1 W(\delta u_i, \Delta u_i; u_i^{(k)}) = & \int_{\Omega_c} \delta u_{i,j} \, \mathcal{L}_{ijkl} \, \Delta u_{l,k} dV \\ + & \int_{\Omega_c} \delta u_{i,j} \, \mathcal{L}_{ijkl} \, u_{k,s} \Delta u_{l,s} dV \\ + & \int_{\Omega_c} \delta u_{i,r} u_{r,j} \, \mathcal{L}_{ijkl} \, u_{k,s} \Delta u_{l,s} dV \\ + & \int_{\Omega_c} \delta u_{i,r} u_{r,j} \, \mathcal{L}_{ijkl} \, \Delta u_{l,k} dV \end{aligned} \tag{16}$$

Similarly, by observing symmetry of the second Piola–Kirchhoff stress tensor S_{ij} we can write

$$\Delta^2 W(\delta u_i, \Delta u_i; u_i^{(k)}) = \int_{\Omega_c} \delta u_{i,l} \Delta u_{l,j} \, S_{ij} dV \tag{17}$$

The weak form of equilibrium expressions for internal (W^{int}) and external (W^{ext}) virtual work, with the above mentioned symmetry of S_{ij} can be written as

$$W^{int}(\delta u_i, {}^{n+1}_{\;\;0}u_i^{(k)}) = \int_{\Omega_c} \delta u_{i,j} \, S_{ij} dV + \int_{\Omega_c} \delta u_{i,r} u_{r,j} \, S_{ij} dV \tag{18}$$

$$W^{ext}(\delta u_i) \;\; = \;\; - \int_{\Omega_c} \rho_0 \, \delta u_i b_i \, dV - \int_{\partial \Omega_c} \delta u_i \, t_i \, dS \tag{19}$$

Standard finite element discretization of the displacement field is:

$$u_i \approx \hat{u}_i = H_I \bar{u}_{Ii} \tag{20}$$

where $\hat{u}_i$ is the approximation displacement field u_i, H_I are FEM shape functions and $\bar{u}_{Ii}$ are nodal displacements. With this approximation, we have:

$$\begin{aligned}
\Delta^1 W(\delta u_i, \Delta u_i; u_i^{(k)}) = & \int_{\Omega_c} (H_{I,j}\delta\bar{u}_{Ii}) \; \mathcal{L}_{ijkl} \; (H_{Q,k}\Delta\bar{u}_{Ql})\, dV \\
+ & \int_{\Omega_c} (H_{I,j}\delta\bar{u}_{Ii}) \; \mathcal{L}_{ijkl} \; (H_{J,k}\bar{u}_{Js})\,(H_{Q,s}\Delta\bar{u}_{Ql})\, dV \\
+ & \int_{\Omega_c} (H_{I,r}\delta\bar{u}_{Ii})\,(H_{J,j}\bar{u}_{Jr})\,\mathcal{L}_{ijkl} \; (H_{J,k}\bar{u}_{Js})\,(H_{Q,s}\Delta\bar{u}_{Ql})\, dV \\
+ & \int_{\Omega_c} (H_{I,r}\delta\bar{u}_{Ii})\,(H_{J,j}\bar{u}_{Jr})\,\mathcal{L}_{ijkl} \; (H_{Q,k}\Delta\bar{u}_{Ql})\, dV
\end{aligned} \tag{21}$$

$$\Delta^2 W(\delta u_i, \Delta u_i; u_i^{(k)}) = \int_{\Omega_c} (H_{I,l}\delta\bar{u}_{Ii})\,(H_{Q,j}\Delta\bar{u}_{Ql})\, S_{ij} dV \tag{22}$$

$$W^{int}(\delta u_i, {}^{n+1}_{0}u_i^{(k)}) = \int_{\Omega_c} (H_{I,j}\delta\bar{u}_{Ii}) \; S_{ij} dV + \int_{\Omega_c} (H_{I,r}\delta\bar{u}_{Ii}) \; (H_{J,j}\bar{u}_{Jr}) \; S_{ij} dV \tag{23}$$

$$W^{ext}(\delta u_i) \;\; = \;\; -\int_{\Omega_c} \rho_0 \; (H_I\delta\bar{u}_{Ii}) \; b_i \; dV - \int_{\partial\Omega_c} (H_I\delta\bar{u}_{Ii}) \; t_i \; dS \tag{24}$$

Upon noting that virtual nodal displacements δu_{Ii} are any non–zero, continuous displacements, and since they occur in all expressions for linearized virtual work, they can be factored out and after some rearengement can be written as (while remembering that $\Delta^1 W + \Delta^1 W + W^{ext} + W^{int} = 0$):

$$\begin{aligned}
& \left(\int_{\Omega_c} H_{I,j}\mathcal{L}_{ijkl}H_{Q,k} dV + \int_{\Omega_c} H_{I,j}\mathcal{L}_{ijkl}H_{J,k}\bar{u}_{Js}H_{Q,s} dV + \right. \\
+ & \int_{\Omega_c} H_{I,r}H_{J,j}\bar{u}_{Jr}\mathcal{L}_{ijkl}H_{J,k}\bar{u}_{Js}H_{Q,s} dV \\
+ & \left. \int_{\Omega_c} H_{I,r}H_{J,j}\bar{u}_{Jr}\mathcal{L}_{ijkl}H_{Q,k} dV + \int_{\Omega_c} H_{I,l}H_{Q,j}S_{ij} dV \right) \Delta\bar{u}_{Ql} \\
+ & \int_{\Omega_c} (H_{I,j}) \; S_{ij} dV + \int_{\Omega_c} (H_{I,r}) \; (H_{J,j}\bar{u}_{Jr}) \; S_{ij} dV \\
= & \int_{\Omega_c} \rho_0 \; (H_I) \; b_i \; dV + \int_{\partial\Omega_c} (H_I) \; t_i \; dS
\end{aligned} \tag{25}$$

The global algorithmic tangent stiffness matrix (tensor) is given as

$$\begin{aligned}
\mathbf{K}_t = & \quad \frac{\partial(\Delta W(\delta u_i, \Delta u_i; u_i^{(k)}))}{\partial(\Delta u_i)} \\
= & \quad \int_{\Omega_c} H_{I,j}\mathcal{L}_{ijkl}H_{Q,k} dV + \int_{\Omega_c} H_{I,j}\mathcal{L}_{ijkl}H_{J,k}\bar{u}_{Js}H_{Q,s} dV \\
& + \int_{\Omega_c} H_{I,r}H_{J,j}\bar{u}_{Jr}\mathcal{L}_{ijkl}H_{J,k}\bar{u}_{Js}H_{Q,s} dV \\
& + \int_{\Omega_c} H_{I,r}H_{J,j}\bar{u}_{Jr}\mathcal{L}_{ijkl}H_{Q,k} dV + \int_{\Omega_c} H_{I,l}H_{Q,j}S_{ij} dV
\end{aligned} \tag{26}$$

The global algorithmic tangent stiffness matrix contains both the linear strain incremental stiffness matrix and the nonlinear geometric and initial stress incremental stiffness matrix. The vector of externally applied load is then

$$\mathbf{R} = \int_{\Omega_c} \rho_0 \ (H_I) \ b_i \ dV + \int_{\partial\Omega_c} (H_I) \ t_i \ dS \tag{27}$$

while the load vector from element stresses is given as

$$\mathbf{F} = \int_{\Omega_c} (H_{I,j}) \ S_{ij} dV + \int_{\Omega_c} (H_{I,r}) \ (H_{J,j} \bar{u}_{Jr}) \ S_{ij} dV \tag{28}$$

It is important to note that the algorithmic tangent stiffness tensor, vector of externally applied loads, and the vector of element stresses are second and fourth order tensor. Conversion from tensors to matrices and vectors is performed by the assembly functions. It is also important to note that the tensor of unknown displacements $\Delta\bar{u}_{Ql}$ is flattened to a one dimensional vector (Δu_i) through proper implementation. The iterative change in displacement vector Δu_i is obtained by setting the linearized virtual work to zero

$$W(\delta u_i, u_i^{(k+1)}) = 0 \ \Rightarrow \ W(\delta u_i, u_i^{(k)}) = -\Delta W(\delta u_i, \Delta u_i; u_i^{(k)}) \tag{29}$$

In particular, the choice of the undeformed configuration Ω_0 for a computational domain $(\Omega_c = \Omega_0)$ yields the Total Lagrangian (TL) formulation. The iterative displacement Δu_i is obtained from the equation

$$W(\delta u_i, {}^{n+1}u_i^{(k)}) = -\Delta W(\delta u_i, \Delta u_i; {}^{n+1}u_i^{(k)}) \tag{30}$$

where

$$\begin{aligned} W(\delta u_i, {}^{n+1}u_i^{(k)}) \ &= \ \int_{\Omega_c} \hat{E}_{ij}(\delta u_i, {}^{n+1}u_i^{(k)}) \ {}^{n+1}S_{ij}^{(k)} \ dV \\ &\quad - \int_{\Omega_c} \rho_0 \ \delta u_i \ {}^{n+1}b_i \ dV - \int_{\partial\Omega_c} \delta u_i \ {}^{n+1}t_i \ dS \end{aligned} \tag{31}$$

and

$$\begin{aligned} \Delta W(\delta u_i, \Delta u_i; {}^{n+1}u_i^{(k)}) \ &= \ \int_{\Omega_c} \hat{E}_{ij}(\delta u_i, {}^{n+1}u_i^{(k)}) \ {}^{n+1}\mathcal{L}_{ijkl}^{(k)} \ \hat{E}_{kl}(\Delta u_i, {}^{n+1}u_i^{(k)}) \ dV \\ &\quad + \int_{\Omega_c} d\hat{E}_{ij}(\delta u_i, \Delta u_i) \ {}^{n+1}S_{ij}^{(k)} \ dV \end{aligned} \tag{32}$$

In the case of hyperelastic–plastic response, the second Piola–Kirchhoff stress ${}^{n+1}S_{ij}^{(k)}$ is obtained by integrating the constitutive law, described in section 3. It should be noted that by performing the integrations in the intermediate configuration, we obtain the Mandel stress ${}^{n+1}\bar{T}_{ij}$ and subsequently the second Piola–Kirchhoff stress $\bar{S}_{kj} = \left(\bar{C}_{ik}\right)^{-1} \bar{T}_{ij}$. The ATS tensor $\bar{\mathcal{L}}_{ijkl}$ is then obtained based on $\bar{S}_{kj}$. In order to obtain the second Piola–Kirchhoff stress S_{kj} and ATS tensor in the initial configuration we need to perform a pull-back from the intermediate configuration to the initial state

$$ {}^{n+1}S_{ij} = {}^{n+1}F^p_{ip} \; {}^{n+1}F^p_{jq} \; {}^{n+1}\bar{S}_{pq} \tag{33} $$

$$ {}^{n+1}\mathcal{L}_{ijkl} = {}^{n+1}F^p_{im} \; {}^{n+1}F^p_{jn} \; {}^{n+1}F^p_{kr} \; {}^{n+1}F^p_{ls} \; {}^{n+1}\bar{\mathcal{L}}_{mnrs} \tag{34} $$

The formulation presented above is rather general and relevant to a large set of engineering solids, both isotropic and anisotropic. This generality will be further enhanced in section 3 with general, constitutive level computations that can handle both isotropic and general anisotropic materials.

3 Finite Deformation Hyperelasto–Plasticity

3.1 Hyperelasticity

A material is called *hyperelastic* or *Green elastic*, if there exists an *elastic potential function* W, also called the *strain energy function per unit volume of the undeformed configuration*, which represents a scalar function of strain of deformation tensors, whose derivatives with respect to a strain component determines the corresponding stress component. The most general form of the elastic potential function, is described in equation (35), with restriction to pure mechanical theory, by using the *axiom of locality* and the *axiom of entropy production*[2]:

$$ W = W\left(X_K, F_{kK}\right) \tag{35} $$

By using the *axiom of material frame indifference*[3], we conclude that W depends only on X_K and C_{IJ}, that is:

$$ W = W\left(X_K, C_{IJ}\right) \quad \text{or:} \quad W = W\left(X_K, c_{ij}\right) \tag{36} $$

[2]See Marsden and Hughes [31] pp. 190.

[3]See Marsden and Hughes [31] pp. 194.

In the case of material isotropy, the strain energy function $W\left(X_K, C_{IJ}\right)$ belongs to the class of isotropic, invariant scalar functions. It satisfies the relation:

$$W\left(X_K, C_{KL}\right) = W\left(X_K, Q_{KI} C_{IJ} \left(Q_{JL}\right)^t\right) \tag{37}$$

where Q_{KI} is the proper orthogonal transformation. If we choose $Q_{KI} = R_{KI}$, where R_{KI} is the orthogonal rotation transformation, defined by the polar decomposition theorem in equation (see Malvern [30]), then:

$$W\left(X_K, C_{KL}\right) = W\left(X_K, U_{KL}\right) = W\left(X_K, v_{kl}\right) \tag{38}$$

Right and left stretch tensors, U_{KL}, v_{kl} have the same principal values (principal stretches) $\lambda_i \quad ; \quad i = \overline{1,3}$ so the strain energy function W can be represented in terms of principal stretches, or similarly in terms of principal invariants of the deformation tensor:

$$W = W\left(X_K, \lambda_1, \lambda_2, \lambda_3, \right) = W\left(X_K, I_1, I_2, I_3\right) \tag{39}$$

where:

$$\begin{aligned} I_1 &\stackrel{\text{def}}{=} C_{II} \\ I_2 &\stackrel{\text{def}}{=} \frac{1}{2}\left(I_1^2 - C_{IJ} C_{JI}\right) \\ I_3 &\stackrel{\text{def}}{=} \det\left(C_{IJ}\right) = \frac{1}{6} e_{IJK} e_{PQR} C_{IP} C_{JQ} C_{KR} = J^2 \end{aligned} \tag{40}$$

Left Cauchy–Green tensors is defined as $C_{IJ} = (F_{kI})^t F_{kJ}$, and the spectral decomposition theorem (see Simo and Taylor [49]) for symmetric positive definite tensors states that $C_{IJ} = \lambda_A^2 \left(N_I^{(A)} N_J^{(A)}\right)_A$ where $A = \overline{1,3}$ and N_I are the eigenvectors ($\|N_I\| = 1$) of C_{IJ}. We can then calculate roots (λ_A^2) of the characteristic polynomial

$$P(\lambda_A^2) \stackrel{\text{def}}{=} -\lambda_A^6 + I_1\, \lambda_A^6 - I_2\, \lambda_A^4 + I_3 = 0 \tag{41}$$

It should be noted that no summation is implied over indices in parenthesis. For example, in the present case $N_I^{(A)}$ is the A–th eigenvector with members $N_1^{(A)}$, $N_2^{(A)}$ and $N_3^{(A)}$, so that the actual equation $C_{IJ} = \lambda_A^2 \left(N_I^{(A)} N_J^{(A)}\right)_A$ can also be written as $C_{IJ} = \sum_{A=1}^{A=3} \lambda_{(A)}^2 N_I^{(A)} N_J^{(A)}$. In order to follow the consistency of indicial notation in this work, we shall make an effort to represent all the tensorial equations in indicial form.

The mapping of the eigenvectors is given by

$$\lambda_{(A)}\, n_i^{(A)} = F_{iJ}\, N_J^{(A)} \tag{42}$$

where $\|n_i^{(A)}\| \equiv 1$. The spectral decomposition of F_{iJ}, R_{iJ} and b_{ij} is then given by

$$F_{iJ} = \lambda_A \left(n_i^{(A)} N_J^{(A)} \right)_A \tag{43}$$

$$R_{iJ} = \sum_{A=1}^{3} n_i^{(A)} N_J^{(A)} \tag{44}$$

$$b_{ij} = \lambda_A^2 \left(n_i^{(A)} n_j^{(A)} \right)_A \tag{45}$$

Recently, Ting [53] and Morman [33] have used Serrin's representation theorem in order to devise a useful representation for generalized strain tensors E_{IJ} through C_{IJ}^m. After some tensor algebra the Lagrangian eigendyad $N_I^{(A)} N_J^{(A)}$, can be written as

$$N_I^{(A)} N_J^{(A)} = \lambda_{(A)}^2 \frac{C_{IJ} - \left(I_1 - \lambda_{(A)}^2 \right) \delta_{IJ} + I_3 \lambda_{(A)}^{-2} (C^{-1})_{IJ}}{2\lambda_{(A)}^4 - I_1 \lambda_{(A)}^2 + I_3 \lambda_{(A)}^{-2}} \tag{46}$$

It should be noted that the denominator in equation (46) can be written as:

$$2\lambda_{(A)}^4 - I_1 \lambda_{(A)}^2 + I_3 \lambda_{(A)}^{-2} = \left(\lambda_{(A)}^2 - \lambda_{(B)}^2 \right) \left(\lambda_{(A)}^2 - \lambda_{(C)}^2 \right) \stackrel{\text{def}}{=} D_{(A)} \tag{47}$$

where indices A, B, C are cyclic permutations of $1, 2, 3$. It follows directly from the definition of $D_{(A)}$ in equation (47) that $\lambda_1 \neq \lambda_2 \neq \lambda_3 \Rightarrow D_{(A)} \neq 0$ for equation (46) to be valid. Similarly we can obtain:

$$(C^{-1})_{IJ} = \lambda_A^{-2} \left(N_I^{(A)} N_J^{(A)} \right)_A \tag{48}$$

The most general form of the isotropic strain energy function W in terms of of principal stretches can be expressed as:

$$W = W\left(X_K, \lambda_1, \lambda_2, \lambda_3, \right) \tag{49}$$

In order to obtain the second Piola–Kirchhoff stress tensor S_{IJ} (and other stress measures) it is necessary to calculate the gradient $\partial W/\partial C_{IJ}$. Moreover, the material tangent stiffness tensor $\mathcal{L}_{IJKL}$ require second order derivatives of the strain energy function $\partial^2 W/(\partial C_{IJ}\, \partial C_{KL})$. In order to obtain these quantities we introduce a second order tensor $M_{IJ}^{(A)}$

$$\begin{aligned} M_{IJ}^{(A)} &\stackrel{\text{def}}{=} \lambda_{(A)}^{-2}\, N_I^{(A)}\, N_J^{(A)} \\ &= (F_{iI})^{-1} \left(n_i^{(A)} n_j^{(A)}\right) (F_{jJ})^{-t} \\ &= \frac{1}{D_{(A)}} \left(C_{IJ} - \left(I_1 - \lambda_{(A)}^2\right)\delta_{IJ} + I_3 \lambda_{(A)}^{-2} (C^{-1})_{IJ}\right) \quad \text{from (46)} \end{aligned} \tag{50}$$

where $D_{(A)}$ was defined by equation (47). With $M_{IJ}^{(A)}$ defined by equation (50), we obtain

$$C_{IJ} = \lambda_A^4 \left(M_{IJ}^{(A)}\right)_A \tag{51}$$

and it also follows

$$(C^{-1})_{IJ} = M_{IJ}^{(1)} + M_{IJ}^{(2)} + M_{IJ}^{(3)} \tag{52}$$

It can also be concluded that:

$$\delta_{IJ} = \lambda_{(1)}^2 M_{IJ}^{(1)} + \lambda_{(2)}^2 M_{IJ}^{(2)} + \lambda_{(3)}^2 M_{IJ}^{(3)} = \lambda_A^2 \left(M_{IJ}^{(A)}\right)_A \tag{53}$$

since, from the orthogonal properties of eigenvectors

$$\delta_{IJ} = \sum_{A=1}^{3} N_I^{(A)}\, N_J^{(A)} = \left(N_I^{(A)}\right)_A \left(N_J^{(A)}\right)_A \tag{54}$$

We also define the *Simo–Serrin* fourth order tensor $\mathcal{M}_{IJKL}$ as:

$$\begin{aligned} \mathcal{M}_{IJKL}^{(A)} &\stackrel{\text{def}}{=} \frac{\partial M_{IJ}^{(A)}}{\partial C_{KL}} = \\ & \frac{1}{D_{(A)}} \left(I_{IJKL} - \delta_{KL}\delta_{IJ} + \lambda_{(A)}^2 \left(\delta_{IJ}\, M_{KL}^{(A)} + M_{IJ}^{(A)}\, \delta_{KL}\right) + \right. \\ &+ I_3 \lambda_{(A)}^{-2} \left((C^{-1})_{IJ}(C^{-1})_{KL} + \frac{1}{2}\left((C^{-1})_{IK}(C^{-1})_{JL} + (C^{-1})_{IL}(C^{-1})_{JK}\right)\right) - \\ &- \left. \lambda_{(A)}^{-2}\, I_3 \left((C^{-1})_{IJ}\, M_{KL}^{(A)} + M_{IJ}^{(A)}\, (C^{-1})_{KL}\right) - D'_{(A)}\, M_{IJ}^{(A)}\, M_{KL}^{(A)}\right) \end{aligned} \tag{55}$$

A complete derivation of $\mathcal{M}_{IJKL}$ is given by Simo and Taylor [49].

We can then define hyperelastic stress measures as

- 2. Piola–Kirchhoff stress tensor $S_{IJ} = 2\frac{\partial W}{\partial C_{IJ}}$

- Mandel stress tensor $T_{IJ} = C_{IK} S_{KJ}$
- 1. Piola–Kirchhoff stress tensor $P_{iJ} = S_{IJ}(F_{iI})^t$
- Kirchhoff stress tensor $\tau_{ab} = F_{aI}(F_{bJ})^t S_{IJ}$

where

$$\begin{aligned} \frac{\partial W(\lambda_{(A)})}{\partial C_{IJ}} &= \frac{\partial^{vol} W(\lambda_{(A)})}{\partial C_{IJ}} + \frac{\partial^{iso} W(\lambda_{(A)})}{\partial C_{IJ}} \\ &= \frac{1}{2} \frac{\partial^{vol} W(J)}{\partial J} J \, (C^{-1})_{IJ} + \frac{1}{2} \, w_A \, (M^{(A)}_{IJ})_A \end{aligned} \tag{56}$$

and

$$w_A = -\frac{1}{3} \frac{\partial^{iso} W(\tilde{\lambda}_{(A)})}{\partial \tilde{\lambda}_B} \tilde{\lambda}_B + \frac{\partial^{iso} W(\tilde{\lambda}_{(A)})}{\partial \tilde{\lambda}_{(A)}} \tilde{\lambda}_{(A)} \tag{57}$$

The tangent stiffness operator is defined as

$$\mathcal{L}_{IJKL} = {}^{vol}\mathcal{L}_{IJKL} + {}^{iso}\mathcal{L}_{IJKL} \tag{58}$$

with

$$\begin{aligned} &{}^{vol}\mathcal{L}_{IJKL} = \\ &J^2 \frac{\partial^{2vol} W(J)}{\partial J \partial J} (C^{-1})_{KL} (C^{-1})_{IJ} + J \frac{\partial^{vol} W(J)}{\partial J} (C^{-1})_{KL} (C^{-1})_{IJ} + 2J \frac{\partial^{vol} W(J)}{\partial J} I^{(C^{-1})}_{IJKL} \end{aligned} \tag{59}$$

$${}^{iso}\mathcal{L}_{IJKL} = Y_{AB} \, (M^{(B)}_{KL})_B \, (M^{(A)}_{IJ})_A + 2 \, w_A \, (\mathcal{M}^{(A)}_{IJKL})_A \tag{60}$$

3.2 Multiplicative Decomposition

Multiplicative decomposition of the deformation gradient is used as a kinematical basis for the developments described here. The motivation for the multiplicative decomposition can be traced back to the early works of Bilby et al. [3], and Kröner [23] on micromechanics of crystal dislocations and application to continuum modeling. In the context of large deformation elastoplastic computations, the work by Lee and Liu [26], Fox [14] and Lee [25] generated an early interest in multiplicative decomposition.

The appropriateness of multiplicative decomposition technique for soils may be justified from the particulate nature of the material. From the micromechanical point of view, plastic deformation in soils arises from slipping, crushing, yielding and plastic bending[4] of granules or platelets comprising the assembly[5]. It can certainly be argued that deformations in soils are predominantly plastic, however, reversible deformations could develop from the elasticity of individual soil grains, and could be relatively large, when particles are locked in high density specimens.

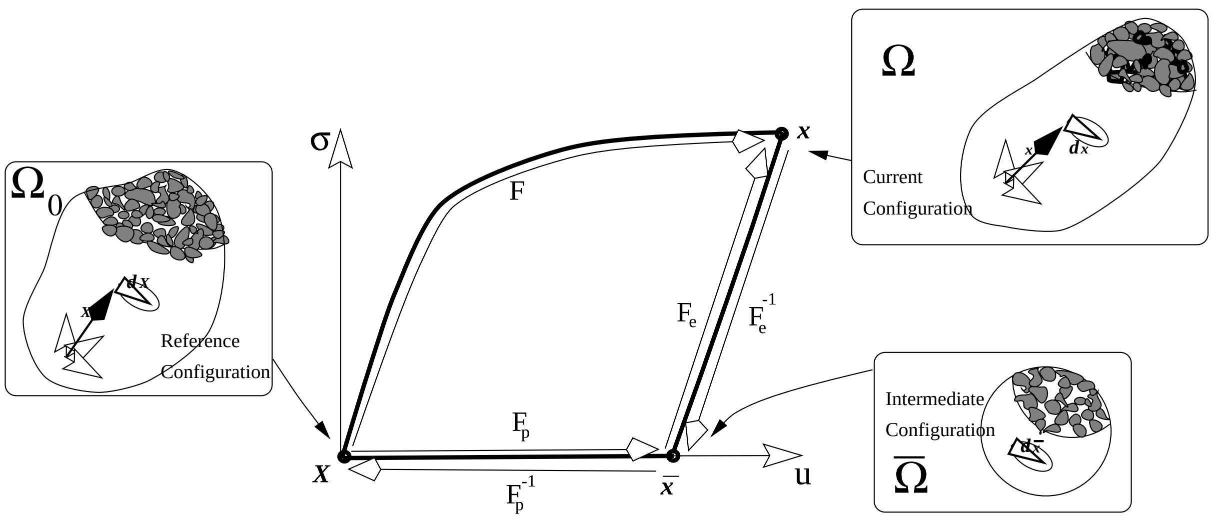

Figure 2: Multiplicative decomposition of deformation gradient: schematics.

The reasoning behind multiplicative decomposition is a rather simple one. If an infinitesimal neighborhood of a body $x_i, x_i + dx_i$ in an inelastically deformed body is cut–out and unloaded to an unstressed configuration, it would be mapped into $\hat{x}_i, \hat{x}_i + d\hat{x}_i$. The transformation would be comprised of a rigid body displacement[6] and purely elastic unloading. The elastic unloading is fictitious, since in materials with a strong Baushinger's effect unloading will lead to loading in another stress direction, and if there are residual stresses, the body must be cut–out in small pieces, and then every piece relieved of stresses. The unstressed

[4]For plate like clay particles.

[5]See also Borja and Alarcòn [5] and Lambe and Whitman [24].

[6]Translation and rotation.

configuration is thus incompatible and discontinuous. The position $\hat{x}_i$ is arbitrary, and we may assume a linear relationship between dx_i and $d\hat{x}_i$, in the form[7]:

$$d\hat{x}_k = (F^e_{ik})^{-1}\, dx_i \tag{61}$$

where $(F^e_{ik})^{-1}$ is not to be understood as a deformation gradient, since it may represent the incompatible, discontinuous deformation of a body. By considering the reference configuration of a body dX_i, then the connection to the current configuration is:

$$dx_k = F_{ki} dX_i \Rightarrow d\hat{x}_k = (F^e_{ik})^{-1}\, F_{ij} dX_j \tag{62}$$

so that one can define:

$$F^p_{kj} \overset{def}{=} (F^e_{ik})^{-1}\, F_{ij} \Rightarrow F_{ij} \overset{\text{def}}{=} F^e_{ki} F^p_{kj} \tag{63}$$

The plastic part of the deformation gradient, F^p_{kj} represents micro–mechanically, the irreversible process of slipping, crushing dislocation and macroscopically the irreversible plastic deformation of a body. The elastic part, F^e_{ki} represents micro–mechanically a pure elastic reversal of deformation for the particulate assembly, macroscopically a linear elastic unloading toward a stress free state of the body, not necessarily a compatible, continuous deformation but rather a fictitious elastic unloading of small cut outs of a deformed particulate assembly or continuum body,

3.3 Constitutive Relations

We propose the free energy density W, which is defined in the intermediate configuration $\bar{\Omega}$, as

$$\rho_0 W(\bar{C}^e_{ij}, \kappa_\alpha) = \rho_0 W^e(\bar{C}^e_{ij}) + \rho_0 W^p(\kappa_\alpha) \tag{64}$$

where $W^e(\bar{C}^e_{ij})$ represents a suitable hyperelastic model in terms of the elastic right deformation tensor $\bar{C}^e_{ij}$, whereas $W^p(\kappa_\alpha)$ represents the hardening. The pertinent dissipation inequality becomes:

$$D = \bar{T}_{ij}\, \bar{L}^p_{ij} + \sum_\alpha \bar{K}_\alpha\, \dot{\kappa}_\alpha \geq 0 \tag{65}$$

[7]referred to same Cartesian coordinate system.

where $\bar{T}_{ij}$ is the Mandel stress and $\bar{L}^p_{ij}$ is the plastic velocity gradient defined on $\bar{\Omega}$. We now define the elastic domain $\mathcal{B}$ as

$$\mathcal{B} = \{\bar{T}_{ij}, \bar{K}_\alpha \mid \Phi(\bar{T}_{ij}, \bar{K}_\alpha) \leq 0\} \tag{66}$$

When yield function Φ is isotropic in $\bar{T}_{ij}$ (which is the case here) in conjunction with elastic isotropy, we can conclude that $\bar{T}_{ij}$ is symmetric and we may replace $\bar{T}_{ij}$ by τ_{ij} in yield function Φ.

As to the choice of an elastic law, it is emphasized that this is largely a matter of convenience, since we shall be dealing with small elastic deformations. Here, the Neo–Hookean elastic law is adopted. The constitutive relations can now be written as

$$\bar{L}^p_{ij} := \dot{F}^p_{ik} \left(F^p_{jk}\right)^{-1} = \dot{\mu}\frac{\partial \Phi^*}{\partial \bar{T}_{ij}} = \dot{\mu}\bar{M}_{ij} \tag{67}$$

$$\bar{K}_\alpha = \bar{K}_\alpha(\bar{\kappa_\beta}) \tag{68}$$

$$\dot{\bar{\kappa}}_\beta = \dot{\mu}\,\frac{\partial \Phi^*}{\partial K_\beta} \quad , \quad \kappa_\beta(0) = 0 \tag{69}$$

where $\bar{K}_\alpha$ $, \alpha = 1, 2, \cdots$ is the "hardening stress", $\Phi^*(\tau_{ij}, \bar{K}_\alpha)$ is the plastic potential, $\bar{\kappa}_\beta$ is internal variables, $\dot{\mu}$ is consistency parameter determined from the loading conditions[8] and $F^p_{ik} = (\bar{F}^e_{li})^{-1} F_{lk}$ is the plastic part of the deformation gradient.

3.4 Implicit Integration Algorithm

The incremental deformation and plastic flow are governed by the system of evolution equations (67) and (69). The flow rule (67) can be integrated to give

$${}^{n+1}F^p_{ij} = \exp\left(\Delta\mu^{n+1}\bar{M}_{ik}\right){}^nF^p_{kj} \tag{70}$$

By using the multiplicative decomposition

$$F_{ij} = \bar{F}^e_{ik}\, F^p_{kj} \Rightarrow \bar{F}^e_{ik} = F_{ij}\ \left(F^p_{kj}\right)^{-1} \tag{71}$$

and equation (70) we obtain

$$\begin{aligned} {}^{n+1}\bar{F}^e_{ij} &= {}^{n+1}F_{im}\ \left({}^nF^p_{mk}\right)^{-1} \exp\left(-\Delta\mu^{n+1}\bar{M}_{kj}\right) \\ &= {}^{n+1}\bar{F}^{e,tr}_{ik} \exp\left(-\Delta\mu^{n+1}\bar{M}_{kj}\right) \end{aligned} \tag{72}$$

[8]These are the Karush–Kuhn–Tucker complementary conditions in the special case of fully associative theory, defining the Standard Dissipative Material, cf. [15].

where we used that

$$ {}^{n+1}\bar{F}^{e,tr}_{ik} = {}^{n+1}F_{im}\ \left({}^{n}F^{p}_{km}\right)^{-1} \tag{73} $$

The elastic deformation is then

$$ \begin{aligned} {}^{n+1}\bar{C}^{e}_{ij} &\stackrel{\text{def}}{=} \left({}^{n+1}\bar{F}^{e}_{im}\right)^{T}\ {}^{n+1}\bar{F}^{e}_{mj} \\ &= \exp\left(-\Delta\mu^{n+1}\bar{M}^{T}_{ir}\right)\ \left({}^{n+1}\bar{F}^{e,tr}_{rk}\right)^{T}\ {}^{n+1}\bar{F}^{e,tr}_{kl}\ \exp\left(-\Delta\mu^{n+1}\bar{M}_{lj}\right) \\ &= \exp\left(-\Delta\mu^{n+1}\bar{M}^{T}_{ir}\right)\ {}^{n+1}\bar{C}^{e,tr}_{rl}\ \exp\left(-\Delta\mu^{n+1}\bar{M}_{lj}\right) \end{aligned} \tag{74} $$

By recognizing that the exponent of a tensor can be expanded in Taylor series[9]

$$ \exp\left(-\Delta\mu^{n+1}\bar{M}_{lj}\right) = \delta_{lj} - \Delta\mu^{n+1}\bar{M}_{lj} + \frac{1}{2}\left(\Delta\mu^{n+1}\bar{M}_{ls}\right)\left(\Delta\mu^{n+1}\bar{M}_{sj}\right) + \cdots \tag{75} $$

and by using the second order expansion in equation (74) and after some tensor algebra we obtain

$$ \begin{aligned} {}^{n+1}\bar{C}^{e}_{ij} = \ & {}^{n+1}\bar{C}^{e,tr}_{rj} - \\ & -\Delta\mu\left({}^{n+1}\bar{M}_{ir}\ {}^{n+1}\bar{C}^{e,tr}_{rj} + {}^{n+1}\bar{C}^{e,tr}_{il}\ {}^{n+1}\bar{M}_{lj}\right) + \\ & +\frac{(\Delta\mu)^2}{2}\left({}^{n+1}\bar{M}_{is}{}^{n+1}\bar{M}_{sr}{}^{n+1}\bar{C}^{e,tr}_{rj} + 2^{n+1}\bar{M}_{ir}{}^{n+1}\bar{C}^{e,tr}_{rl}{}^{n+1}\bar{M}_{lj} + {}^{n+1}\bar{M}_{ls}{}^{n+1}\bar{M}_{sj}{}^{n+1}\bar{C}^{e,tr}_{rl}\right) - \\ & -(\Delta\mu)^3\left(\frac{1}{2}\ {}^{n+1}\bar{M}_{is}{}^{n+1}\bar{M}_{sr}\ {}^{n+1}\bar{C}^{e,tr}_{rl}\ {}^{n+1}\bar{M}_{lj} - \frac{1}{2}\ {}^{n+1}\bar{M}_{ir}\ {}^{n+1}\bar{C}^{e,tr}_{rl}\ {}^{n+1}\bar{M}_{ls}\ \ {}^{n+1}\bar{M}_{sj}\right) + \\ & +\frac{(\Delta\mu)^4}{4}\left({}^{n+1}\bar{M}_{is}{}^{n+1}\bar{M}_{sr}\ {}^{n+1}\bar{C}^{e,tr}_{rl}\ {}^{n+1}\bar{M}_{ls}\ \ {}^{n+1}\bar{M}_{sj}\right) \end{aligned} \tag{76} $$

First order series expansion includes constant and linear (up to $\Delta\mu$) members. Second order expansion includes the complete equation above.

Remark 3.1 The Taylor's series expansion in equation (75) is a proper approximation for the general nonsymmetric tensor $\bar{M}_{lj}$. That is, the approximate solution given by equation (76) is valid for a general anisotropic solid. This contrasts with the spectral decomposition family of solutions[10] which are restricted to isotropic solids.

Remark 3.2 In the limit, when the deformations are sufficiently small, the solution (76) collapses to

$$ \lim_{F_{ij}\to\delta_{ij}} \delta_{ij} + 2^{n+1}\epsilon_{ij} = \ + \ \ \delta_{ij} + 2^{n+1}\epsilon^{e,tr}_{ij} $$

[9] See for example Pearson [37].

[10] See Simo [45].

$$
\begin{aligned}
& - && \Delta\mu^{n+1}\bar{M}_{ij} - 2\Delta\mu^{n+1}\bar{M}_{ir}{}^{n+1}\epsilon^{tr}_{rj} \\
& - && \Delta\mu\ {}^{n+1}\bar{M}_{ij} - 2\Delta\mu\ {}^{n+1}\epsilon^{tr}_{il}\ {}^{n+1}\bar{M}_{lj} \\
& + && \Delta\mu^2\ {}^{n+1}\bar{M}_{il}\ {}^{n+1}\bar{M}_{lj} + 2\Delta\mu^2\ {}^{n+1}\bar{M}_{ir}\ {}^{n+1}\epsilon^{tr}_{rl}{}^{n+1}\bar{M}_{lj} \\
& = && \delta_{ij} + 2^{n+1}\epsilon^{e,tr}_{ij} - 2\Delta\mu\ {}^{n+1}\bar{M}_{ij} \\
\Rightarrow {}^{n+1}\epsilon_{ij} & = && {}^{n+1}\epsilon^{tr}_{ij} - \Delta\mu\ {}^{n+1}\bar{M}_{ij}
\end{aligned}
\tag{77}
$$

which represents a small deformation elastic predictor–plastic corrector equation in strain space. In working out the small deformation counterpart (77) it was used that

$$
\begin{aligned}
\lim_{F_{ij}\to\delta_{ij}} {}^{n+1}\bar{C}^{e}_{ij} &= \delta_{ij} + 2^{n+1}\epsilon_{ij} \\
2\Delta\mu\ {}^{n+1}\epsilon^{tr}_{il}\ {}^{n+1}\bar{M}_{lj} &\ll {}^{n+1}\bar{M}_{ij} \\
\Delta\mu &\ll 1
\end{aligned}
\tag{78}
$$

By neglecting the higher order term with $\Delta\mu^2$ in equation (76), the solution for the right elastic deformation tensor ${}^{n+1}\bar{C}^{e}_{ij}$ can be written as

$$
{}^{n+1}\bar{C}^{e}_{ij} = {}^{n+1}\bar{C}^{e,tr}_{ij} - \Delta\mu\ \left({}^{n+1}\bar{M}_{ir}\ {}^{n+1}\bar{C}^{e,tr}_{rj}\ + {}^{n+1}\bar{C}^{e,tr}_{il}\ {}^{n+1}\bar{M}_{lj}\right) \tag{79}
$$

The hardening rule (69) can be integrated to give

$$
{}^{n+1}\kappa_{\alpha} = {}^{n}\kappa_{\alpha} + \Delta\mu\ \left.\frac{\partial\Phi^*}{\partial K_{\alpha}}\right|_{n+1} \tag{80}
$$

The incremental problem is defined by equations (79), (80), the constitutive relations

$$
{}^{n+1}\bar{S}_{IJ} = 2\left.\frac{\partial W}{\partial C_{IJ}}\right|_{n+1} \tag{81}
$$

$$
{}^{n+1}K_{\alpha} = -\left.\frac{\partial W}{\partial \kappa_{\alpha}}\right|_{n+1} \tag{82}
$$

and the Karush–Kuhn–Tucker (KKT) conditions

$$
\Delta\mu < 0 \quad ; \quad {}^{n+1}\Phi \leq 0 \quad ; \quad \Delta\mu\ {}^{n+1}\Phi = 0 \tag{83}
$$

where

$$
\Phi = \Phi(\bar{T}_{ij}, K_{\alpha}) \tag{84}
$$

Remark 3.3 The Mandel stress tensor $\bar{T}_{ij}$ can be obtained from the second Piola–Kirchhoff stress tensor $\bar{S}_{kj}$ and the right elastic deformation tensor $\bar{C}^e_{ik}$ as $\bar{T}_{ij} = \bar{C}^e_{ik}\ \bar{S}_{kj}$

This set of nonlinear equations will be solved with a Newton type procedure, described below. For a given ${}^{n+1}F_{ij}$, or ${}^{n+1}\bar{C}^{e,tr}_{ij}$, the upgraded quantities ${}^{n+1}\bar{S}_{IJ}$ and ${}^{n+1}K_\alpha$ can be found, then the appropriate pull–back to Ω_0 or push–forward to Ω will give ${}^{n+1}S_{IJ}$ and ${}^{n+1}\tau_{ij}$

$$ {}^{n+1}S_{IJ} = \left({}^{n+1}F^p_{iI}\right)^{-1}\ {}^{n+1}\bar{S}_{IJ}\ \left({}^{n+1}F^p_{jJ}\right)^{-T} \tag{85} $$

$$ {}^{n+1}\tau_{ij} = {}^{n+1}\bar{F}^e_{iI}\ {}^{n+1}\bar{S}_{IJ}\ \left({}^{n+1}F^e_{jJ}\right)^{-1} \tag{86} $$

The elastic predictor, plastic corrector equation

$$ {}^{n+1}\bar{C}^e_{ij} = {}^{n+1}\bar{C}^{e,tr}_{ij} - \Delta\mu\ {}^{n+1}Z_{ij} \tag{87} $$

is used as a starting point for a Newton iterative algorithm. In the previous equation, we have introduced tensor Z_{ij}

$$ Z_{ij} \ = \ \Delta\mu \left({}^{n+1}\bar{M}_{ir}\ {}^{n+1}\bar{C}^{e,tr}_{rj} + {}^{n+1}\bar{C}^{e,tr}_{il}\ {}^{n+1}\bar{M}_{lj}\right) - \tag{88} $$

The definition of Z_{ij} above assumes use of first order expansion in (76). The trial right–elastic deformation tensor is defined as

$$ {}^{n+1}\bar{C}^{e,tr}_{ij} = \left({}^{n+1}\bar{F}^{e,tr}_{ri}\right)^T\ \left({}^{n+1}\bar{F}^{e,tr}_{rj}\right) = \left({}^{n+1}F_{rM}\ \left({}^{n}F^p_{iM}\right)^{-1}\right)^T\ \left({}^{n+1}F_{rS}\ \left({}^{n}F^p_{jS}\right)^{-1}\right) \tag{89} $$

We introduce a tensor of deformation residuals

$$ R_{ij} = \underbrace{\bar{C}^e_{ij}}_{current} - \underbrace{\left({}^{n+1}\bar{C}^{e,tr}_{ij} - \Delta\mu\ {}^{n+1}Z_{ij}\right)}_{BackwardEuler} \tag{90} $$

The tensor R_{ij} represents the difference between the current right–elastic deformation tensor and the Backward Euler right elastic deformation tensor. The trial right–elastic deformation tensor ${}^{n+1}\bar{C}^{e,tr}_{ij}$ is maintained fixed during the iteration process. The first order Taylor series expansion can be applied to the tensor of residuals R_{ij} in order to obtain the iterative change, the new residual R^{new}_{ij} from the old R^{old}_{ij}

$$ R^{new}_{ij} = R^{old}_{ij} + d\bar{C}^e_{ij} + d(\Delta\mu)\ {}^{n+1}Z_{ij} + \Delta\mu \frac{\partial\, {}^{n+1}Z_{ij}}{\partial \bar{T}_{mn}}\ d\bar{T}_{mn} + \Delta\mu \frac{\partial\, {}^{n+1}Z_{ij}}{\partial K_\alpha}\ dK_\alpha \tag{91} $$

Furthermore, since

$$\bar{T}_{mn} = \bar{C}^e_{mk}\,\bar{S}_{kn} \quad\Rightarrow\quad \left(\bar{C}^e_{sk}\right)^{-1}\,\bar{T}_{sn} = \bar{S}_{kn} \tag{92}$$

we can write

$$\begin{aligned} d\bar{T}_{mn} &= d\bar{C}^e_{mk}\,\bar{S}_{kn} + \bar{C}^e_{mk}\,d\bar{S}_{kn} \\ &= d\bar{C}^e_{mk}\,\bar{S}_{kn} + \frac{1}{2}\,\bar{C}^e_{mk}\,\bar{\mathcal{L}}^e_{knpq}\,d\bar{C}^e_{pq} \\ &= d\bar{C}^e_{mk}\,\left(\bar{C}^e_{sk}\right)^{-1}\,\bar{T}_{sn} + \frac{1}{2}\,\bar{C}^e_{mk}\,\bar{\mathcal{L}}^e_{knpq}\,d\bar{C}^e_{pq} \end{aligned} \tag{93}$$

so that after setting $R^{new}_{ij} = 0$ and some tensor algebra we obtain

$$\begin{aligned} 0 = \quad & R^{old}_{ij} + d(\Delta\mu)\,{}^{n+1}Z_{ij} + \Delta\mu\frac{\partial^{n+1}Z_{ij}}{\partial K_\alpha}\,dK_\alpha + \\ + \quad & (\delta_{im}\delta_{nj} + \Delta\mu\frac{\partial^{n+1}Z_{mn}}{\partial\bar{T}_{ik}}\,\left(\bar{C}^e_{sj}\right)^{-1}\,\bar{T}_{sk} + \frac{1}{2}\,\Delta\mu\frac{\partial^{n+1}Z_{mn}}{\partial\bar{T}_{pq}}\,\bar{C}^e_{pk}\,\bar{\mathcal{L}}^e_{kqij}\,)\,d\bar{C}^e_{ij} \end{aligned} \tag{94}$$

Upon introducing the notation

$$\mathcal{T}_{mnij} = \delta_{im}\delta_{nj} + \Delta\mu\frac{\partial^{n+1}Z_{mn}}{\partial\bar{T}_{ik}}\,\left(\bar{C}^e_{sj}\right)^{-1}\,\bar{T}_{sk} + \frac{1}{2}\,\Delta\mu\frac{\partial^{n+1}Z_{mn}}{\partial\bar{T}_{pq}}\,\bar{C}^e_{pk}\,\bar{\mathcal{L}}^e_{kqij} \tag{95}$$

we can solve for $d\bar{C}^e_{ij}$

$$d\bar{C}^e_{pq} = \left(\mathcal{T}_{mnpq}\right)^{-1}\left(-R^{old}_{mn} - d(\Delta\mu)\,{}^{n+1}Z_{mn} - \Delta\mu\frac{\partial^{n+1}Z_{mn}}{\partial K_\alpha}\,dK_\alpha\right) \tag{96}$$

By using that

$$dK_\alpha = \frac{\partial K_\alpha}{\partial\kappa_\beta}\,d\kappa_\beta = -d(\Delta\mu)\,\frac{\partial K_\alpha}{\partial\kappa_\beta}\,\frac{\partial Q}{\partial K_\beta} = -d(\Delta\mu)\,H_{\alpha\beta}\,\frac{\partial Q}{\partial K_\beta} \tag{97}$$

it follows from (96)

$$d\bar{C}^e_{pq} = \left(\mathcal{T}_{mnpq}\right)^{-1}\left(-R^{old}_{mn} - d(\Delta\mu)\,{}^{n+1}Z_{mn} + \Delta\mu\frac{\partial^{n+1}Z_{mn}}{\partial K_\alpha}\,d(\Delta\mu)\,H_{\alpha\beta}\,\frac{\partial Q}{\partial K_\beta}\right) \tag{98}$$

A first order Taylor series expansion of a yield function together with (97) provides

$$\begin{aligned} {}^{new}\Phi(\bar{T}_{ij}, K_\alpha) = \quad & {}^{old}\Phi(\bar{T}_{ij}, K_\alpha) + \\ + \quad & \left(\frac{\partial\Phi(\bar{T}_{ij}, K_\alpha)}{\partial\bar{T}_{pn}}\,\left(\bar{C}^e_{sq}\right)^{-1}\,\bar{T}_{sn} + \frac{1}{2}\,\frac{\partial\Phi(\bar{T}_{ij}, K_\alpha)}{\partial\bar{T}_{mn}}\,\bar{C}^e_{mk}\,\bar{\mathcal{L}}^e_{knpq}\right)\,d\bar{C}^e_{pq} \\ - \quad & d(\Delta\mu)\,\frac{\partial\Phi(\bar{T}_{ij}, K_\alpha)}{\partial K_\alpha}\,H_{\alpha\beta}\,\frac{\partial\Phi^*}{\partial K_\beta} \end{aligned} \tag{99}$$

Upon introducing the following notation

$$\mathcal{F}_{pq} = \frac{\partial \Phi(\bar{T}_{ij}, K_\alpha)}{\partial \bar{T}_{pn}} \left(\bar{C}^e_{sq}\right)^{-1} \bar{T}_{sn} + \frac{1}{2} \frac{\partial \Phi(\bar{T}_{ij}, K_\alpha)}{\partial \bar{T}_{mn}} \bar{C}^e_{mk} \bar{\mathcal{L}}^e_{knpq} \tag{100}$$

and with the solution for $d\bar{C}^e_{pq}$ from (98), (99) becomes

$$\begin{aligned} & {}^{new}\Phi(\bar{T}_{ij}, K_\alpha) = {}^{old}\Phi(\bar{T}_{ij}, K_\alpha) + \\ + \ & \mathcal{F}_{pq} \left((\mathcal{T}_{mnpq})^{-1} \left(-R^{old}_{mn} - d(\Delta\mu)\ {}^{n+1}Z_{mn} + d(\Delta\mu)\ \Delta\mu\ \frac{\partial\, {}^{n+1}Z_{mn}}{\partial K_\alpha}\ H_{\alpha\beta}\ \frac{\partial \Phi^*}{\partial K_\beta} \right) \right) \\ - \ & d(\Delta\mu)\ \frac{\partial \Phi(\bar{T}_{ij}, K_\alpha)}{\partial K_\alpha}\ H_{\alpha\beta}\ \frac{\partial \Phi^*}{\partial K_\beta} \end{aligned} \tag{101}$$

After setting ${}^{new}\Phi(\bar{T}_{ij}, K_\alpha) = 0$ we can solve for the incremental consistency parameter $d(\Delta\mu)$

$$d(\Delta\mu) = \frac{{}^{old}\Phi - \mathcal{F}_{pq}\ (\mathcal{T}_{mnpq})^{-1}\ R^{old}_{mn}}{\mathcal{F}_{pq}\ (\mathcal{T}_{mnpq})^{-1}\ {}^{n+1}Z_{mn} - \Delta\mu\ \mathcal{F}_{pq}\ (\mathcal{T}_{mnpq})^{-1}\ \frac{\partial\, {}^{n+1}Z_{mn}}{\partial K_\alpha}\ H_{\alpha\beta}\ \frac{\partial \Phi^*}{\partial K_\beta} + \frac{\partial \Phi}{\partial K_\alpha}\ H_{\alpha\beta}\ \frac{\partial \Phi^*}{\partial K_\beta}} \tag{102}$$

Remark 3.4 In the limit, for small deformations, the incremental consistency parameter $d(\Delta\mu)$ becomes

$$d(\Delta\mu) = \frac{{}^{old}\Phi - (n_{mn}\ E_{mnpq}) \left(\delta_{pm}\delta_{nq} + \Delta\mu\ \frac{\partial m_{mn}}{\partial \sigma_{ij}}\ E_{ijpq} \right)^{-1} R^{old}_{mn}}{n_{mn}\ E_{mnpq} \left(\delta_{mp}\delta_{qn} + \Delta\mu\ \frac{\partial m_{pq}}{\partial \sigma_{ij}}\ E_{ijmn} \right)^{-1} {}^{n+1}m_{mn} + \frac{\partial \Phi}{\partial K_\alpha}\ H_{\alpha\beta}\ \frac{\partial \Phi^*}{\partial K_\beta}} \tag{103}$$

since in the limit, as deformations become small

$$\begin{aligned} \lim_{F_{ij}\to\delta_{ij}} \mathcal{T}_{mnpq} &= \delta_{pm}\delta_{nq} + \Delta\mu\ \frac{\partial m_{mn}}{\partial \sigma_{ij}}\ E_{ijpq} \\ \lim_{F_{ij}\to\delta_{ij}} \mathcal{F}_{pq} &= \frac{1}{2}\ \frac{\partial \Phi}{\partial \sigma_{mn}}\ E_{mnpq} \\ \lim_{F_{ij}\to\delta_{ij}} Z_{pq} &= 2\ m_{pq} \\ \lim_{F_{ij}\to\delta_{ij}} R_{pq} &= 2\ \epsilon_{pq} \end{aligned} \tag{104}$$

Upon noting that the residual R_{pq} is defined in strain space, the incremental consistency parameter $d(\Delta\mu)$ compares exactly with it's small strain counterpart (Jeremić and Sture [19]).

The procedure described below summarizes the implementation of the return algorithm.

3.4.1 Return Algorithm

Given the right elastic deformation tensor ${}^{n}\bar{C}^{e}_{pq}$ and a set of hardening variables ${}^{n}K_{\alpha}$ at a specific quadrature point in a finite element, we compute the relative deformation gradient ${}^{n+1}f_{ij}$ for a given displacement increment $\Delta^{n+1}u_i$

$$ {}^{n+1}f_{ij} = \delta_{ij} + u_{i,j} \tag{105} $$

and the right deformation tensor

$$ {}^{n+1}\bar{C}^{e,tr}_{ij} = \left({}^{n+1}f_{ir}\ {}^{n}F^{e}_{rk}\right)^T \left({}^{n+1}f_{kl}\ {}^{n}F^{e}_{lj}\right) = \left({}^{n}F^{e}_{rk}\right)^T \left({}^{n+1}f_{ir}\ \right)^T \left({}^{n+1}f_{kl}\ {}^{n}F^{e}_{lj}\right) \tag{106} $$

Then we compute the trial elastic second Piola–Kirchhoff stress and the trial elastic Mandel stress tensor

$$ {}^{n+1}\bar{S}^{e,tr}_{ij} = 2\frac{\partial W}{\partial^{n+1}\bar{C}^{e,tr}_{ij}} \tag{107} $$

$$ {}^{n+1}\bar{T}^{e,tr}_{ij} = {}^{n+1}\bar{C}^{e,tr}_{il}\ {}^{n+1}\bar{S}^{e,tr}_{lj} \tag{108} $$

We then evaluate the yield function ${}^{n+1}\Phi^{tr}(\bar{T}^{e,tr}_{ij}, K_{\alpha})$, and set

$$ \begin{aligned} {}^{n+1}\bar{C}^{e}_{ij} &= {}^{n+1}\bar{C}^{e,tr}_{ij} \\ {}^{n+1}K_{\alpha} &= {}^{n}K_{\alpha} \\ {}^{n+1}T_{ij} &= {}^{n}T^{e,tr}_{ij} \end{aligned} $$

and exit constitutive integration procedure. If ${}^{n+1}\Phi^{tr} \leq 0$ there is no plastic flow in the current increment.

If the yield criterion has been violated (${}^{n+1}\Phi^{tr} > 0$) proceed

step 1. k^{th} iteration. Known variables

$$ {}^{n+1}\bar{C}^{e(k)}_{ij} \quad ; \quad {}^{n+1}\kappa^{(k)}_{\alpha} \quad ; \quad {}^{n+1}K^{(k)}_{\alpha} \quad ; \quad {}^{n+1}T^{(k)}_{ij} \quad ; \quad {}^{n+1}\Delta\mu^{(k)} $$

evaluate the yield function and the residual

$$ \begin{aligned} \Phi^{(k)} &= \Phi({}^{n+1}\bar{T}^{e(k)}_{ij}, {}^{n+1}K^{(k)}_{\alpha}) \\ R^{(k)}_{ij} &= {}^{n+1}\bar{C}^{e,(k)}_{ij} - \left({}^{n+1}\bar{C}^{e,tr}_{ij} - {}^{n+1}\Delta\mu^{(k)n+1}Z^{(k)}_{ij}\right) \end{aligned} $$

step 2. Check for convergence, $\Phi^{(k)} \leq NTOL$ and $\|R^{(k)}_{ij}\| \leq NTOL$. If convergence criterion is satisfied set

$$ {}^{n+1}\bar{C}^{e}_{ij} = {}^{n+1}\bar{C}^{e(k)}_{ij} $$

$$
\begin{aligned}
{}^{n+1}\kappa_\alpha &= {}^{n+1}\kappa_\alpha^{(k)} \\
{}^{n+1}K_\alpha &= {}^{n+1}K_\alpha^{(k)} \\
{}^{n+1}T_{ij} &= {}^{n+1}T_{ij}^{(k)} \\
{}^{n+1}\Delta\mu &= {}^{n+1}\Delta\mu^{(k)}
\end{aligned}
$$

Exit constitutive integration procedure.

step 3.[11] If convergence is not achieved compute the elastic stiffness tensor $\mathcal{L}_{ijkl}$

$$\bar{\mathcal{L}}_{ijkl}^{(k)} = 4 \, \frac{\partial^2 W}{\partial \bar{C}_{ij}^{e(k)} \, \partial \bar{C}_{kl}^{e(k)}} \tag{109}$$

step 4. Compute the incremental consistency parameter $d(\Delta\mu^{(k+1)})$

$$d(\Delta\mu^{(k+1)}) = \frac{\Phi^{(k)} - \bar{\mathcal{F}}_{mn}^{(k)} \, R_{mn}{}^{(k)}}{\bar{\mathcal{F}}_{mn}^{(k)} \, Z_{mn}{}^{(k)} - \Delta\mu^{(k)} \, \bar{\mathcal{F}}_{mn}{}^{(k)} \, \dfrac{\partial Z_{mn}{}^{(k)}}{\partial K_\alpha} \, \bar{H}_\alpha{}^{(k)} + \dfrac{\partial \Phi^{(k)}}{\partial K_\alpha} \, \bar{H}_\alpha{}^{(k)}} \tag{110}$$

where

$$\bar{H}_\alpha{}^{(k)} = H_{\alpha\beta}{}^{(k)} \, \frac{\partial \Phi^{*,(k)}}{\partial K_\beta} \quad ; \quad \bar{\mathcal{F}}_{mn}{}^{(k)} = \mathcal{F}_{pq}{}^{(k)} \, \left(\mathcal{T}_{mnpq}{}^{(k)}\right)^{-1}$$

$$\mathcal{F}_{pq} = \frac{\partial \Phi(\bar{T}_{ij}^{(k)}, K_\alpha^{(k)})}{\partial \bar{T}_{pn}} \, \left(\bar{C}_{sq}^{e,(k)}\right)^{-1} \, \bar{T}_{sn}^{(k)} + \frac{1}{2} \, \frac{\partial \Phi(\bar{T}_{ij}^{(k)}, K_\alpha^{(k)})}{\partial \bar{T}_{mn}} \, \bar{C}_{mk}^{e,(k)} \, \bar{\mathcal{L}}_{knpq}^{e,(k)}$$

$$\mathcal{T}_{mnij} = \delta_{im}\delta_{nj} + \Delta\mu^{(k)} \, \frac{\partial Z_{mn}^{(k)}}{\partial \bar{T}_{ik}^{(k)}} \, \left(\bar{C}_{sj}^{e,(k)}\right)^{-1} \, \bar{T}_{sk}^{(k)} + \frac{1}{2} \, \Delta\mu^{(k)} \, \frac{\partial Z_{mn}^{(k)}}{\partial \bar{T}_{pq}} \, \bar{C}_{pk}^{e,(k)} \, \bar{\mathcal{L}}_{kqij}^{e,(k)}$$

step 5. Update the consistency parameter $\Delta\mu^{(k+1)}$

$$\Delta\mu^{(k+1)} = \Delta\mu^{(k)} + d(\Delta\mu^{(k+1)}) \tag{111}$$

step 6. Calculate the increments for the right deformation tensor, the hardening variable and the Mandel stress

$$
\begin{aligned}
&d\bar{C}_{pq}^{e,(k+1)} = \\
&\left(\mathcal{T}_{mnpq}^{(k)}\right)^{-1} \left(-R_{mn}^{(k)} - d(\Delta\mu^{(k+1)}) \, {}^{n+1}Z_{mn}^{(k)} + \Delta\mu^{(k)} \, \frac{\partial Z_{mn}^{(k)}}{\partial K_\alpha} \, d(\Delta\mu^{(k+1)}) \, \bar{H}_\alpha^{(k)} \right)
\end{aligned} \tag{112}
$$

[11] From step 3. to step 9. all of the variables are in intermediate $n+1$ configuration. For the sake of brevity we are omitting superscript $n+1$.

$$d\kappa_\alpha^{(k+1)} = d(\Delta\mu^{(k+1)})\ \frac{\partial \Phi^{*,(k)}}{\partial K_\beta} \tag{113}$$

$$dK_\alpha^{(k+1)} = -d(\Delta\mu^{(k+1)})\ H_{\alpha\beta}^{(k)}\ \frac{\partial \Phi^{*,(k)}}{\partial K_\beta} \tag{114}$$

$$d\bar{T}_{mn}^{(k+1)} = d\bar{C}_{mk}^{e,(k+1)}\ \left(\bar{C}_{sk}^{e,(k)}\right)^{-1}\ \bar{T}_{sn}^{(k)} + \frac{1}{2}\,\bar{C}_{mk}^{e,(k)}\ \bar{\mathcal{L}}_{knpq}^{e,(k)}\ d\bar{C}_{pq}^{e,(k+1)} \tag{115}$$

step 7. Update the right deformation tensor $\bar{C}_{pq}^{e,(k+1)}$, hardening variable $K_\alpha^{(k+1)}$ and Mandel stress $\bar{T}_{mn}^{(k+1)}$

$$\begin{aligned}
\bar{C}_{pq}^{e,(k+1)} &= \bar{C}_{pq}^{e,(k)} + d(\bar{C}_{pq}^{e,(k+1)}) \\
\kappa_\alpha^{(k+1)} &= \kappa_\alpha^{(k)} + d(\kappa_\alpha^{(k+1)}) \\
K_\alpha^{(k+1)} &= K_\alpha^{(k)} + d(K_\alpha^{(k+1)}) \\
\bar{T}_{mn}^{(k+1)} &= \bar{T}_{mn}^{(k)} + d(\bar{T}_{mn}^{(k+1)})
\end{aligned} \tag{116}$$

step 8. evaluate the yield function and the residual

$$\begin{aligned}
\Phi^{(k+1)} &= \Phi(\bar{T}_{ij}^{e(k+1)}, K_\alpha^{(k+1)}) \\
R_{ij}^{(k+1)} &= \bar{C}_{ij}^{e,(k+1)} - \left(\bar{C}_{ij}^{e,tr} - \Delta\mu^{(k+1)} Z_{ij}^{(k+1)}\right)
\end{aligned} \tag{117}$$

step 9. Set $k = k + 1$ and

$$\begin{aligned}
\Delta\mu^{(k)} &= \Delta\mu^{(k+1)} \\
\bar{C}_{pq}^{e,(k)} &= \bar{C}_{pq}^{e,(k+1)} \\
\kappa_\alpha^{(k)} &= \kappa_\alpha^{(k+1)} \\
K_\alpha^{(k)} &= K_\alpha^{(k+1)} \\
\bar{T}_{mn}^{(k)} &= \bar{T}_{mn}^{(k+1)}
\end{aligned} \tag{118}$$

and return to step 2.

3.5 Algorithmic Tangent Stiffness Tensor

Starting from the elastic predictor–plastic corrector equation

$${}^{n+1}\bar{C}_{ij}^{e} = {}^{n+1}\bar{C}_{ij}^{e,tr} - \Delta\mu\ {}^{n+1}Z_{ij} \tag{119}$$

to which we apply a first order Taylor series expansion to obtain (after some tensor algebra),

$$d\bar{C}^e_{ij} = (\mathcal{T}_{mnij})^{-1} \left(d\bar{C}^{e,tr}_{ij} - d(\Delta\mu)\, Z_{ij} + \Delta\mu\, d(\Delta\mu) \frac{\partial Z_{ij}}{\partial K_\alpha} H_{\alpha\beta} \frac{\partial \Phi^*}{\partial K_\beta} \right) \tag{120}$$

where $\mathcal{T}_{mnij}$ was defined in (95)

Next we use the first order Taylor series expansion of the yield function $d\Phi(\bar{T}_{ij}, K_\alpha) = 0$

$$\frac{\partial \Phi}{\partial \bar{T}_{mn}} d\bar{T}_{mn} + \frac{\partial \Phi}{\partial K_\alpha} dK_\alpha = \mathcal{F}_{pq}\, d\bar{C}^e_{pq} - \frac{\partial \Phi}{\partial K_\alpha} d(\Delta\mu)\, H_{\alpha\beta} \frac{\partial \Phi^*}{\partial K_\beta} = 0 \tag{121}$$

with $\mathcal{F}_{pq}$ defined in (100).

By using the solution for $d\bar{C}^e_{ij}$ from (120) we can write

$$\begin{aligned} \mathcal{F}_{pq}\, (\mathcal{T}_{mnpq})^{-1} \left(d\bar{C}^{e,tr}_{mn} - d(\Delta\mu)\, Z_{mn} + \Delta\mu\, d(\Delta\mu) \frac{\partial Z_{mn}}{\partial K_\alpha} H_{\alpha\beta} \frac{\partial \Phi^*}{\partial K_\beta} \right) & \\ - \frac{\partial \Phi}{\partial K_\alpha} d(\Delta\mu)\, H_{\alpha\beta} \frac{\partial \Phi^*}{\partial K_\beta} &= 0 \end{aligned} \tag{122}$$

We are now in the position to solve for the incremental consistency parameter $d(\Delta\mu)$

$$d(\Delta\mu) = \frac{\mathcal{F}_{pq}\, (\mathcal{T}_{mnpq})^{-1}\, d\bar{C}^{e,tr}_{mn}}{\Gamma} \tag{123}$$

where we have used Γ to denote

$$\Gamma = \mathcal{F}_{pq}\, (\mathcal{T}_{mnpq})^{-1\, n+1} Z_{mn} - \Delta\mu \mathcal{F}_{pq}\, (\mathcal{T}_{mnpq})^{-1} \frac{\partial^{n+1} Z_{mn}}{\partial K_\alpha} H_{\alpha\beta} \frac{\partial \Phi^*}{\partial K_\beta} + \frac{\partial \Phi}{\partial K_\alpha} H_{\alpha\beta} \frac{\partial \Phi^*}{\partial K_\beta} \tag{124}$$

Since

$$d\bar{S}_{kn} = \frac{1}{2}\, \bar{\mathcal{L}}_{knpq}\, d\bar{C}^e_{pq} \tag{125}$$

and by using (120) we can write

$$\begin{aligned} d\bar{C}^e_{pq} = \quad & (\mathcal{T}_{mnpq})^{-1} \left(\delta_{mv}\, \delta_{nt} - \frac{\mathcal{F}_{op}\, (\mathcal{T}_{rsop})^{-1}\, \delta_{rv}\, \delta_{st}}{\Gamma} Z_{mn} + \right. \\ & \left. \Delta\mu \frac{\mathcal{F}_{op}\, (\mathcal{T}_{rsop})^{-1}\, \delta_{rv}\, \delta_{st}}{\Gamma} \frac{\partial Z_{ij}}{\partial K_\alpha} H_{\alpha\beta} \frac{\partial \Phi^*}{\partial K_\beta} \right) d\bar{C}^{e,tr}_{vt} \end{aligned} \tag{126}$$

Then

$$d\bar{C}^e_{pq} = \bar{\mathcal{P}}_{pqvt}\, d\bar{C}^{e,tr}_{vt} \tag{127}$$

where

$$\bar{\mathcal{P}}_{pqvt} = (\mathcal{T}_{mnpq})^{-1} \left(\delta_{mv}\delta_{nt} - \frac{\mathcal{F}_{ab}(\mathcal{T}_{vtab})^{-1}}{\Gamma} \left(Z_{mn} - \Delta\mu \, \frac{\partial^{n+1}Z_{mn}}{\partial K_\alpha} H_{\alpha\beta} \frac{\partial \Phi^*}{\partial K_\beta}\right)\right) \tag{128}$$

The algorithmic tangent stiffness tensor $\bar{\mathcal{L}}^{ATS}_{ijkl}$ (in intermediate configuration $\bar{\Omega}$) is then defined as

$$\bar{\mathcal{L}}^{ATS}_{knvt} = \bar{\mathcal{L}}^{e}_{knpq} \, \bar{\mathcal{P}}_{pqvt} \tag{129}$$

Pull–back to the reference configuration Ω_0 yields the algorithmic tangent stiffness tensor $\mathcal{L}_{ijkl}$ in the reference configuration Ω_0

$${}^{n+1}\mathcal{L}^{ATS}_{ijkl} = {}^{n+1}F^p_{im} \; {}^{n+1}F^p_{jn} \; {}^{n+1}F^p_{kr} \; {}^{n+1}F^p_{ls} \; {}^{n+1}\bar{\mathcal{L}}^{ATS}_{mnrs} \tag{130}$$

Remark 3.5 In the limit, for small deformations and isotropic response, the Algorithmic Tangent Stiffness tensor $\mathcal{L}^{ATS}_{ijkl}$ becomes

$$\lim_{F_{ij}\to\delta_{ij}} \bar{\mathcal{L}}^{ATS}_{vtpq} = E^{ATS}_{vtpq} = \mathcal{R}_{knvt} - \frac{n_{cd}\mathcal{R}_{cdvt}\mathcal{R}_{knmr}\mathcal{H}_{mr}}{\Gamma}$$

since

$$\lim_{F_{ij}\to\delta_{ij}} \bar{\mathcal{T}}_{mnpq} = \Upsilon_{mnpq} = \delta_{pm}\delta_{nq} + \Delta\mu \frac{\partial m_{mn}}{\partial \sigma_{rs}} E^e_{kspq}$$

$$\lim_{F_{ij}\to\delta_{ij}} \mathcal{F}_{ab} = \frac{1}{2} n_{cd} E^e_{cdab}$$

$$\lim_{F_{ij}\to\delta_{ij}} \mathcal{H}_{mn} = m_{mn} - \Delta\mu \frac{\partial m_{mn}}{\partial K_\alpha} H_{\alpha\beta} \frac{\partial \Phi^*}{\partial K_\beta}$$

$$\lim_{F_{ij}\to\delta_{ij}} \Gamma = n_{ab}\mathcal{R}_{abmn}\mathcal{H}_{mn} + \frac{\partial \Phi}{\partial K_\alpha} H_{\alpha\beta} \frac{\partial \Phi^*}{\partial K_\beta}$$

It is noted that the Algorithmic Tangent Stiffness tensor given by (131) compares exactly with it's small strain counterpart (Jeremić and Sture [19]).

3.6 Material Model

A large deformation material model used in computations is briefly described here. The model relies on the development behind the so called MRS–Lade model (Sture et al. [51])

and is subsequently denoted the B–Model. The B–Model is a single surface model, with uncoupled cone portion and cap portion hardening. Very low confinement region was carefully modeled and the yield surface was shaped in such a way to mimic recent findings obtained during Micro Gravity Mechanics tests aboard Space Shuttle (Sture et al. [50]). The large deformation model definition is based on the use of the Mandel stress $\bar{T}_{ij}$ for describing yield and potential surfaces. A detailed description of the model is given by Jeremić et al. [18].

4 Numerical Simulations of Micro Gravity Mechanics

In this section we present numerical modeling of low confinement, microgravity large deformation triaxial test performed during Space Shuttle STS–79 mission in September 1996. Figure 3 shows load–displacement and volume–displacement data for three low confinement tests. The response curves represent load–displacement data as they were measured during the experiments. The signal contains significant noise and the presented data are in raw form. The elastic response appears to be very stiff (from unloading–reloading loops). Detailed description of the experimental setup is given by Sture et al. [50].

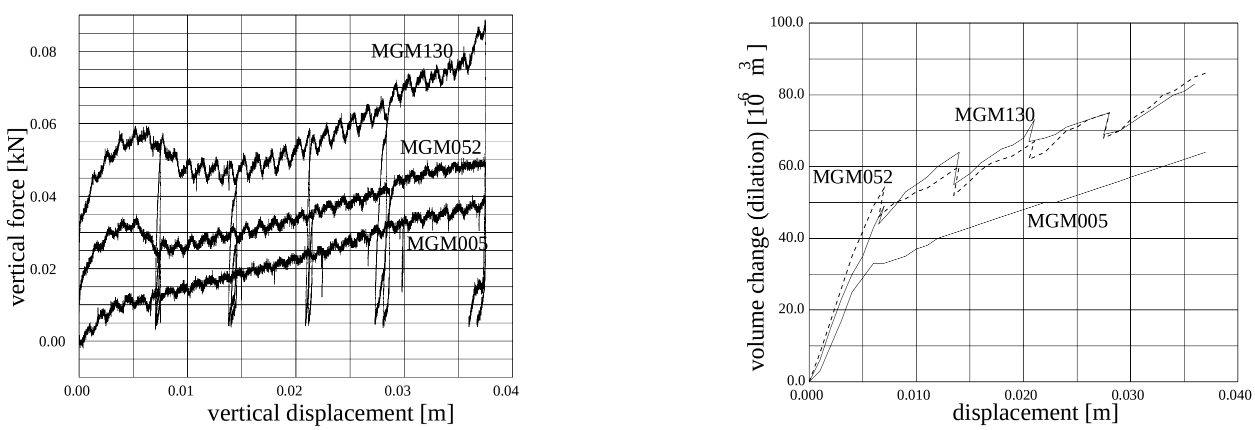

Figure 3: Micro Gravity Mechanics, load displacement and volume displacement curves for the three tests.

The three–dimensional finite element mesh used to model the MGM test is depicted in Figures 4. Instead of developing two dimensional finite element formulation, we have opted for a full three dimensional implementation. Although the state of stress is triaxial, we model the experiments with a 3D model. Six quadratic 20–node brick elements where

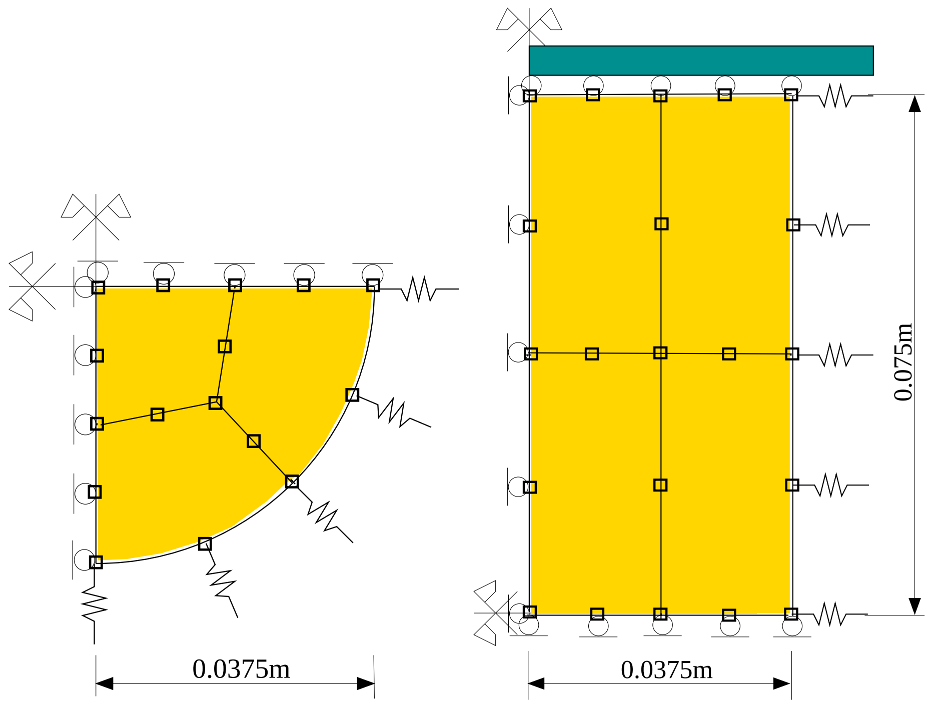

Figure 4: Finite element mesh for the MGM specimen.

chosen to model one–eighth of the specimen. The analysis was performed in two stages. First stage involved isotropic compression to the design pressure. For the first stage only symmetry displacement boundary conditions were in place. Influence of the membrane was removed, since the membrane does not have significant stiffness in compression, and membrane prestressing had a minor effect at this stage. During this stage the response was purely hyperelastic.

After the the first stage, the displacement boundary conditions were changed by adding the movable boundary at the top. The top movable boundary applied displacements to the top nodes by means of equivalent forces, obtained through the partial inversion of a stiffness matrix. The membrane influence was modeled by adding equivalent stiffness (springs) to the boundary nodes. Instead of using thin, highly distorted brick elements (membrane is $0.3mm$, distortion ratio would be $(2*37.5mm*\pi/8)/(0.3mm) \approx 100/1)$. we opted for the equivalent spring method. The output from the one element extension tests on the hyperelastic latex rubber specimen where used to form a non–linear spring of appropriate stiffness. Consistent integration of the stiffness terms for the quadratic brick element then supplied equivalent spring stiffness. Special attention was given to the specimen ends, where the latex membrane was wrapped around the end platen and created a ring in the horizontal plane (parallel to end platen) which was stiffer than the unstretched membrane surrounding the specimen. The last row of nodes was thus supported by stiffer equivalent membrane elements. The material parameters for the B Material Model for all three confining pressures[12] were kept the same except for the Young's modulus. This consistency in material parameters is important, since all three specimens contained the same Ottawa F-75 sand at 85% relative density.

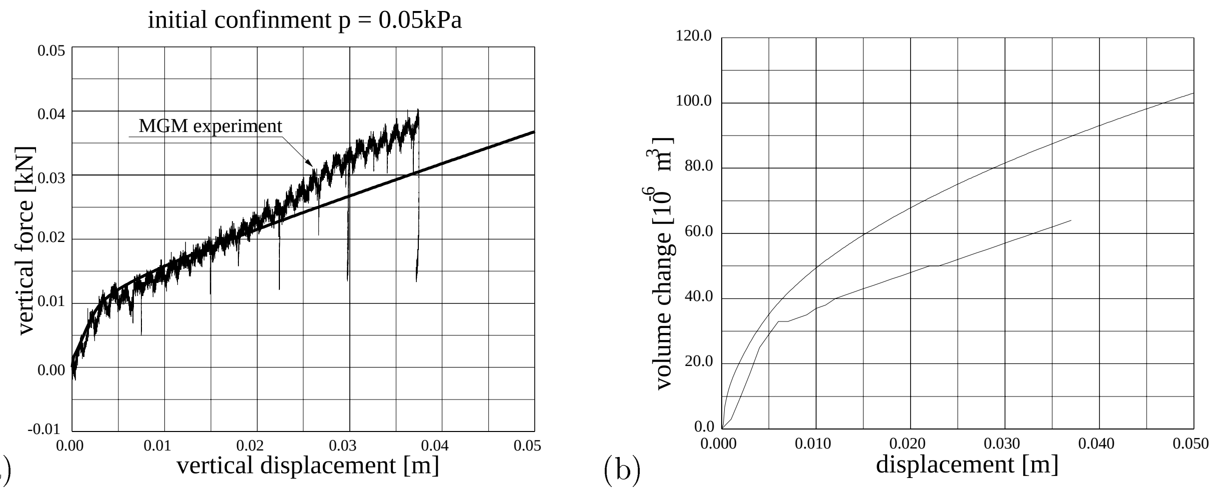

(a) (b)

Figure 5: Mechanics of granular materials responses, initial confinement ($p_0 = 0.05kPa$) test (a) load–deformation and (b) volume–deformation experiments and numerical results.

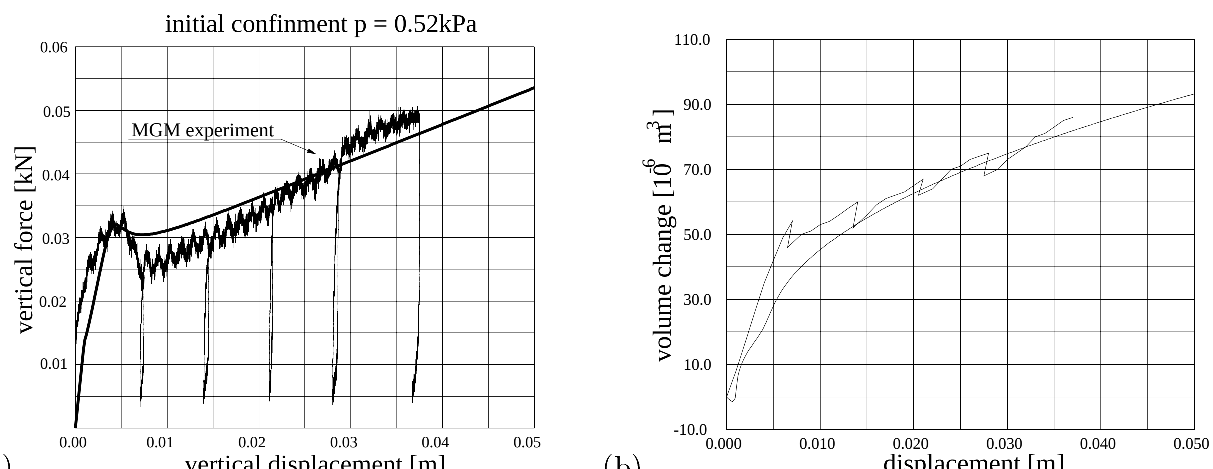

(a) (b)

Figure 6: Mechanics of granular materials responses, initial confinement ($p_0 = 0.52kPa$) test (a) load–deformation and (b) volume–deformation experiments and numerical results.

[12] $E = 300.0; 360.0; 700.0\ kN/m^2$; $\nu = 0.2$; $p_c = 1000.0\ kN/m^2$; $p_t = 0.0\ kN/m^2$; $n = 0.2$; $a = 5.0$; $b = 0.707$; $\eta_{init} = 2.5$; $b_1 = 1.0$; $d_{hard} = 5000.0$; $e_{hard} = 0.5$; $\eta_{res} = 0.15$; $\eta_{peak} = 1.75$; $\eta_{start} = 0.25$; $l = 1.0$; $c_{cone} = 0.030$; $r = 1.00$; $c_{cap} = 0.30$; $p_{c,0} = 1000.0\ kN/m^2$; $a_s = 100.0$; $b_s = 0.707$)

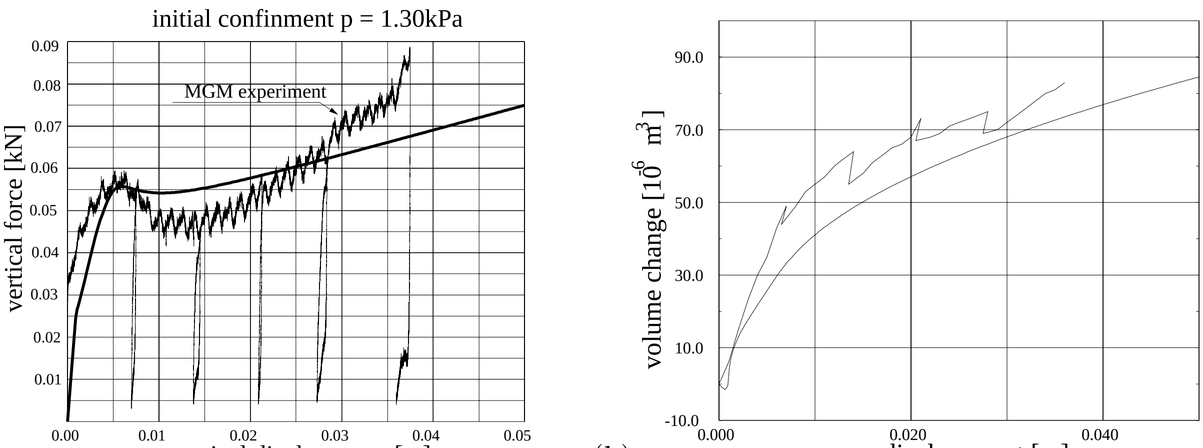

(a) (b)

Figure 7: Mechanics of granular materials responses, initial confinement ($p_0 = 1.30kPa$) test (a) load–deformation and (b) volume–deformation experiments and numerical results.

Figures 5(a), 6(a) and 7(a) show comparison of numerical modeling with the test data for load–displacement. Following observations are made. The initial (elastic) stiffness is higher in the actual experiments. The peak strength is modeled quite accurately, while the post–peak behavior is slightly stiffer in the numerical experiment. The residual stiffness is softer in the numerical model than observed in the MGM tests. This can be explained by the stiffer specimen ends in a physical test. In other words, the latex membrane wrapped around the end platens (the end platens are 30% wider than the specimen) usually sticks to the end platen after some radial displacements and then acts as a full restraint. The friction between end platens and the sand specimen can also add to the whole specimen stiffness, however, the end platens were made of highly polished tungsten–carbide, which has a very low friction angle with quartz sand (3°), and we have thus decided to neglect the influence of end platen friction on the overall response. It is of interest to note that the maximum mobilized friction angle is in the range of 70° and the dilatancy angles observed in the early parts of the experiments are 30°, which is unusually high.

Figures 5(b), 6(b) and 7(b) shows comparison of volumetric–displacement data for experiments and numerical modeling. In modeling the lowest confinement ($p_0 = 0.05kPa$) level we correctly predict complete lack of volumetric compression. Numerical predictions for two other confinements ($p_0 = 0.52kPa$, $p_0 = 1.20kPa$) shows small amount of initial volume compression which was not observed in experiments. Figure 8 shows a typical specimen before and after the test. The latex ring formed by wrapping of membrane around end platens is visible on both specimen ends.

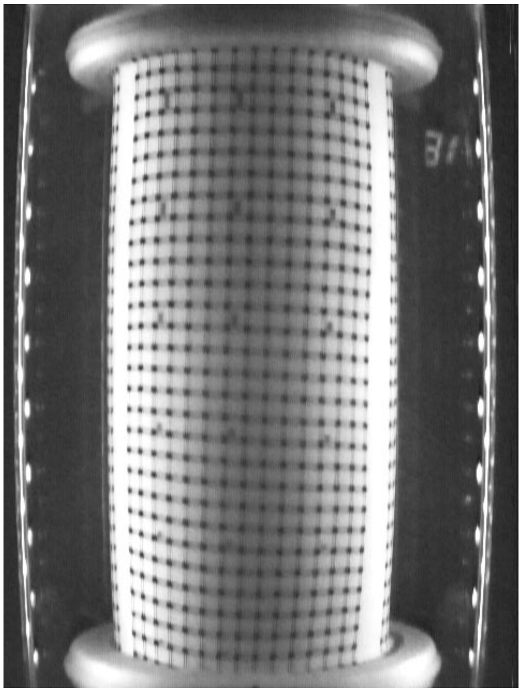

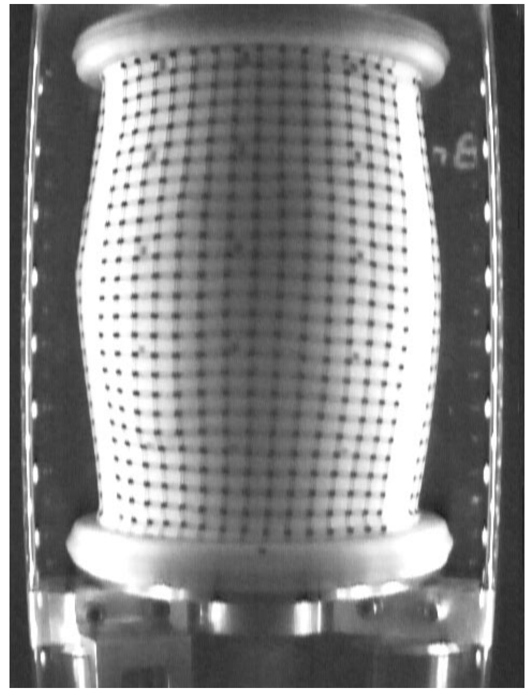

Figure 8: The specimen ($p = 1.30\ kPa$) before and after the test.

The effect of the latex membrane on the load displacement behavior of specimen cannot be neglected for the low confinement experiments. As a triaxial specimen expands, the membrane expands as well. The stretching of the hyperelastic membrane produces additional stresses and increase the original confinement level. Figures 9, 10 and 11 shows the influence of latex membrane on the specimen behavior. The response without latex membrane is softer, and it does not level off in the post peak region. The load displacement response has a flat portion, but starts hardening after approximately 15% axial deformation for two higher confinement tests ($p = 0.52\ kPa$ and $p = 1.30\ kPa$), while for the the very low confinement test ($p = 0.05\ kPa$) it hardens monotonically. This can be explained by the large displacement effects. For large axial deformations, lateral bulging is significant. As the axial deformation progresses, the material (sand) moves from the specimen center to the boundary region, thus creating a slight hardening effect. The increase in peak strength due to the latex membrane effects is not too pronounced. The post peak region, however, shows additional stiffening. For the lowest confinement test, the influence of the membrane is substantial since the specimen itself (at only $p = 0.05\ kPa$) is quite soft.

Figure 12 depicts the deformed shape of a specimen. Without the latex membrane, the

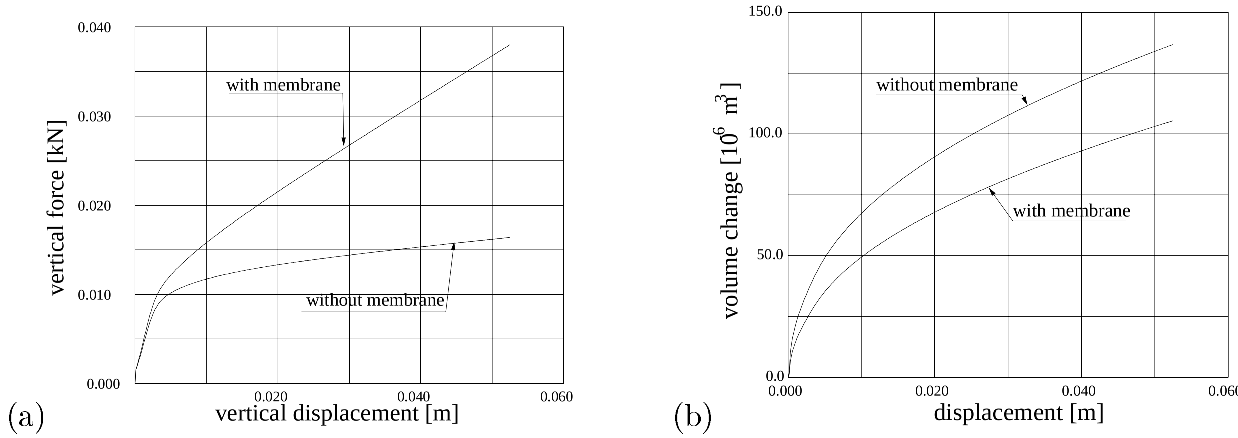

Figure 9: Mechanics of granular materials responses, initial confinement ($p_0 = 0.05kPa$) (a) load–deformation and (b) volume–deformation numerical predictions. Influence of latex membrane on the overall response.

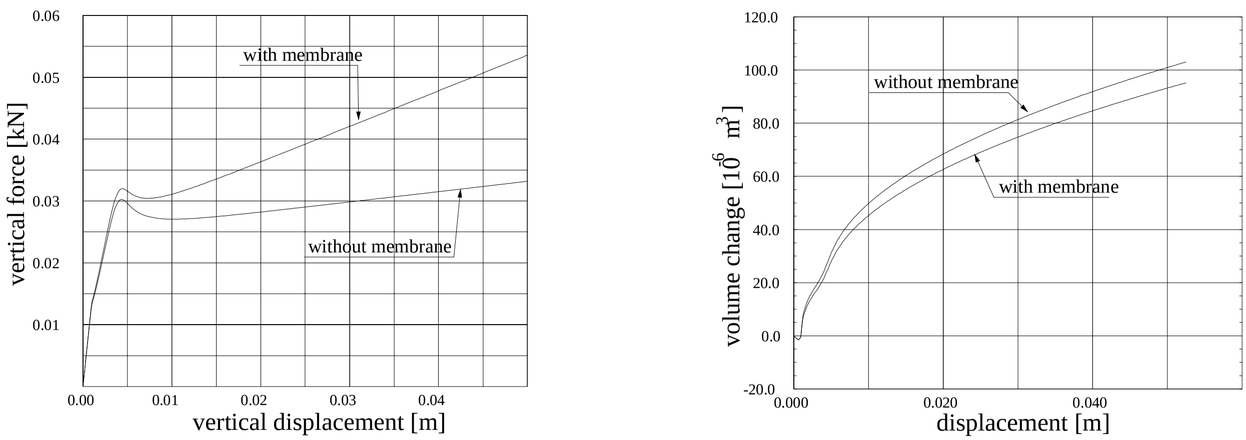

Figure 10: Mechanics of granular materials responses, initial confinement ($p_0 = 0.52kPa$) (a) load–deformation and (b) volume–deformation numerical predictions. Influence of latex membrane on the overall response.

specimen deforms uniformly. The above mentioned end restraint results in a diffuse bulging deformed shape, shown in Figure 12.

5 Concluding Remarks

In this paper we have presented a new large deformation constitutive formulation for geomaterials. Constitutive formulation was used in conjunction with large deformation Lagrangian finite element method. The formulation is capable of simulating large deformation hyperelastic–plastic behavior of geomaterials, even when collinearity between eigentriads of

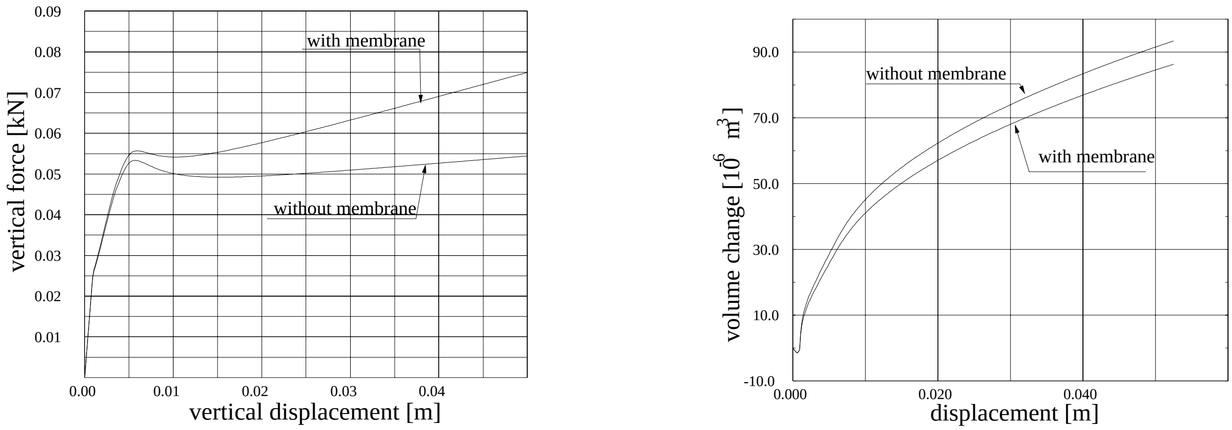

Figure 11: Mechanics of granular materials responses, initial confinement ($p_0 = 1.30kPa$) (a) load–deformation and (b) volume–deformation numerical predictions. Influence of latex membrane on the overall response.

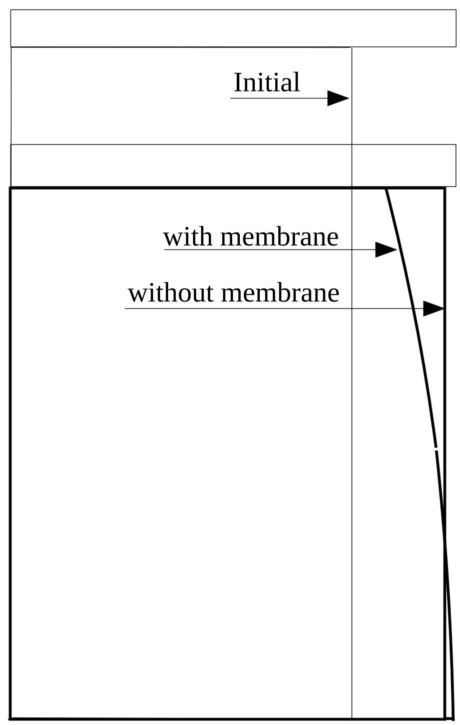

Figure 12: Uniform and bulging deformed shape of a specimen.

stress and strains is lost (for anisotropic and cyclic response). A detailed constitutive formulation has been presented. Moreover, the return algorithm was outlined with implementation details. The developed formulation and implementation were used to simulate large deformation tests on sand performed under very low confinement. To this end, a consistent set of material parameters for the B material model was used to accurately simulate three low confinement tests. It was shown that the latex membrane has substantial influence on the behavior of sand specimen at very low confinement pressures.

Acknowledgment

Partial support by NASA Grant NAS8-38779 from Marshall Space Flight Center is greatfully acknowledged.

References

[1] ARMERO, F. Formulation and finite element implementation of a multiplicative model of coupled poro–plasticity at finite strains under fully saturated conditions. *International Journal for Computer Methods in Applied Mechanics and Engineering 171* (1999), 205–241.

[2] BATHE, K., SLAVKOVIĆ, R., AND KOJIĆ, M. On large strain elasto–plastic and creep analysis. In *Finite Element Methods for Nonlinear Problems, Europe–US Symposium, Trondheim, Norway* (1985), W. Bergan, Bathe, Ed., pp. 176–190.

[3] BILBY, B. A., GARDNER, L. R. T., AND STROH, A. N. Continuous distributions of dislocations and the theory of plasticity. In *IX^e Congrès International de Mèchanique Appliquèe* (Universitè de Bruxelles, 50. Avènue Franklin Roosevelt, 1957), vol. VIII, pp. 35–44.

[4] BORJA, R. I. Cam – clay plasticity, part1: Implicit integration of constitutive equation based on a nonlinear elastic stress predictor. *Computer Methods in Applied Mechanics and Engineering 88* (1991), 225–240.

[5] BORJA, R. I., AND ALARCÓN, E. A mathematical framework for finite strain elasto-plastic consolidation part 1: Balance laws, variational formulation, and linearization. *Computer Methods in Applied Mechanics and Engineering 122* (1995), 145–171.

[6] BORJA, R. I., AND LEE, S. R. Cam–clay plasticity, part I: Implicit integration of elasto–plastic constitutive relations. *Computer Methods In Applied Mechanics and Engineering 78* (1990), 49–72.

[7] BORJA, R. I., AND TAMAGNINI, C. Cam–clay plasticity part iii: Extension of the infinitesimal model to include finite strains. *International Journal for Computer Methods in Applied Mechanics and Engineering 155* (1998), 73–95.

[8] BORJA, R. I., TAMAGNINI, C., AND ALARCÓN, E. Elastoplastic consolidation at finite strain part 2: Finite element implementation and numerical examples. *International Journal for Computer Methods in Applied Mechanics and Engineering 159* (1998), 103–122.

[9] Crisfield, M. A. Consistent schemes for plasticity computation with the Newton Raphson method. *Computational Plasticity Models, Software, and Applications 1* (1987), 136–160.

[10] Cuitiño, A., and Ortiz, M. A material – independent method for extending stress update algorithms from small–strain plasticity to finite plasticity with multiplicative kinematics. *Engineering Computations 9* (1992), 437–451.

[11] de Borst, R., and Feenstra, P. H. Studies in anysotropic plasticity with reference to the hill criterion. *International Journal for Numerical Methods in Engineering 29* (1990), 315–336.

[12] Eterovic, A. L., and Bathe, K.-J. A hyperelastic – based large strain elasto – plastic constitutive formulation with combined isotropic – kinematic hardening using the logarithmic stress and strain measures. *International Journal for Numerical Methods in Engineering 30* (1990), 1099–1114.

[13] Famiglietti, C. M., and Prevost, J. H. Solution of the slump test using a finite deformation elasto–plastic drucker–prager model. *International Journal for Numerical Methods in Engineering 37* (1994), 3869–3903.

[14] Fox, N. On the continuum theories of dislocations and plasticity. *Quarterly Journal of Mechanics and Applied Mathematics XXI*, 1 (1968), 67–75.

[15] Halphen, B., and Son, N. Q. Sur les matériaux standards généralisés. *Journal De Méchanique 14*, 1 (1975), 39–63.

[16] Hibbitt, H. D., Marcal, P. V., and Rice, J. R. A finite element formulation for problems of large strain and large displacements. *International Journal of Solids and Structures 6* (1970), 1069–1086.

[17] Hill, R. *The Mathematical Theory of Plasticity*, 1st. ed. The Oxford Engineering Science Series. Oxford at the Clarendon Press, 1950.

[18] Jeremić, B., Runesson, K., and Sture, S. A model for elastic–plastic pressure sensitive materials subjected to large deformations. *International Journal of Solids and Structures 36*, 31/32 (1999), 4901–4918.

[19] Jeremić, B., and Sture, S. Implicit integrations in elasto–plastic geotechnics. *International Journal of Mechanics of Cohesive–Frictional Materials 2* (1997), 165–183.

[20] Kojić, M., and Bathe, K.-J. The "effective stress function" algorithm for thermo elasto plasticity and, creep. *International Journal for Numerical Methods in Engineering 24* (1987), 1509–1532.

[21] Kojić, M., and Bathe, K.-J. Studies of finite element procedures – stress solution of a closed elastic strain path with stretching and shearing using the updated lagrangian jaumann formulation. *Computers and Structures 26*, 1/2 (1987), 175–179.

[22] Krieg, R. D., and Krieg, D. B. Accuracies of numerical solution methods for the elastic - perfectly plastic model. *Journal of Pressure Vessel Technology* (November 1977), 510–515.

[23] Kröner, E. Algemeine kontinuumstheorie der versetzungen und eigenspanungen. *Archive for Rational Mechanics and Analysis 4*, 4 (1960), 273–334.

[24] Lambe, W. T., and Whitman, R. V. *Soil Mechanics, SI Version.* John Wiley and Sons, 1979.

[25] Lee, E. H. Elastic–plastic deformation at finite strains. *Journal of Applied Mechanics 36*, 1 (1969), 1–6.

[26] Lee, E. H., and Liu, D. T. Finite–strain elastic–plastic theory with application to plane–wave analysis. *Journal of Applied Physics 38*, 1 (January 1967), 19–27.

[27] Lewis, R. W., and Khoei, A. R. Numerical modeling of large deformation in metal powder forming. *International Journal for Computer Methods in Applied Mechanics and Engineering 159* (1998), 291–328.

[28] Liu, C. H., Wong, J. Y., and Mang, H. A. Large strain finite element analysis of sand: model, algorithm and application to numerical simulations of tire–sand interaction. *Computers and Structures 159* (1999), 253–265.

[29] Lubarda, V. A., and Lee, E. H. A correct definition of elastic and plastic deformation and its computational significance. *Journal of Applied Mechanics 48* (1981), 35–40.

[30] MALVERN, L. E. *Introduction to the Mechanics of a Continuous Medium.* In Engineering of the Physical Sciences. Prentice Hall Inc., 1969.

[31] MARSDEN, J. E., AND HUGHES, T. J. R. *Mathematical Foundations of Elasticity.* Prentice Hall Inc,, 1983. local CM65; 4QA 931.M42 ; ISBN 0-13-561076-1.

[32] MCMEEKING, R. M., AND RICE, J. R. Finite – element formulations for problems of large elastic – plastic deformation. *International Jopurnal of SOlids and Structures 11* (1975), 601–616.

[33] MORMAN, K. N. The generalized strain meassures with application to nonhomogeneous deformation in rubber–like solids. *Journal of Applied Mechanics 53* (1986), 726–728.

[34] NAGTEGAAL, J. C., AND DE JONG, J. E. Some aspects of non–isotropic workhardening in finite strain plasticity. In *Plasticity of Metals at finite strains*, E. H. Lee and R. L. Mallet, Eds. Stanford University, 1981, pp. 65–106.

[35] ORTIZ, M., AND POPOV, E. P. Accuracy and stability of integration algorithms for elastoplastic constitutive relations. *International Journal for Numerical Methods in Engineering 21* (1985), 1561–1576.

[36] ORTIZ, M., AND SIMO, J. C. An analysis of a new class of integration algorithms for elastoplastic, constitutive relations. *International Journal for Numerical Methods in Engineering 23* (1986), 353–366.

[37] PEARSON, C. E., Ed. *Handbook of Applied Mathematics.* Van Nostrand Reinhold Company, 1974.

[38] PERIĆ, D., AND DE SOUZA NETO, E. A. A new computational model for Tresca plasticity at finite strains with an optimal parametrization in the principal space. *International Journal for Computer Methods in Applied Mechanics and Engineering 159* (1998), 463–489.

[39] PERIĆ, D., OWEN, D. R. J., AND HONNOR, M. E. A model for finite strain elasto–plasticity based on logarithmic strains: Computational issues. *Computer Methods in Applied Mechanics and Engineering 94* (1992), 35–61.

[40] Runesson, K., and Samuelsson, A. Aspects on numerical techniques in small deformation plasticity. In *NUMETA 85 Numerical Methods in Engineering, Theory and Applications* (1985), G. N. P. J. Middleton, Ed., AA.Balkema., pp. 337–347.

[41] Runesson, K., Sture, S., and Willam, K. Integration in computational plasticity. *Computers & Structures 30*, 1/2 (1988), 119–130.

[42] Saran, M. J., and Runesson, K. A generalized closest–point–projection method for deformation–neutralized formualtion in finite strain plasticity. *Engineering Computations 9* (1992), 359–370.

[43] Simo, J. C. A framework for finite strain elastoplasticity based on maximum plastic dissipation and the multiplicative decomposition: Part i. continuum formulation. *Computer Methods in Applied Mechanics and Engineering 66* (1988), 199–219. TA345. C6425.

[44] Simo, J. C. A framework for finite strain elastoplasticity based on maximum plastic dissipation and the multiplicative decomposition: Part ii. computational aspects. *Computer Methods in Applied Mechanics and Engineering 68* (1988), 1–31. TA345. C6425.

[45] Simo, J. C. Algorithms for static and dynamic multiplicative plasticity that preserve the classical return mapping schemes of the infinitesimal theory. *Computer Methods in Applied Mechanics and Engineering 99* (1992), 61–112.

[46] Simo, J. C., and Meschke, G. A new class of algorithms for classical plasticity extended to finite strain. application to geomaterials. *Computational Mechanics 11* (1993), 253–278.

[47] Simo, J. C., and Ortiz, M. A unified approach to finite deformation elastoplastic analysis based on the use of hyperelastic constitutive equations. *Computer Methods in Applied Mechanics and Engineering 49* (1985), 221–245.

[48] Simo, J. C., and Taylor, R. L. Consistent tangent operators for rate-independent elastoplasticity. *Computer Methods in Applied Mechanics and Engineering 48* (1985), 101–118.

[49] Simo, J. C., and Taylor, R. L. Quasi–incompressible finite elasticity in principal stretches. continuum basis and numerical algorithms. *Computer Methods in Applied Mechanics and Engineering 85* (1991), 273–310.

[50] Sture, S., Costes, N., Batiste, S., Lankton, M., AL-Shibli, K., Jeremić, B., Swanson, R., and Frank, M. Mechanics of granular materials at low effective stresses. *ASCE Journal of Aerospace Engineering 11*, 3 (July 1998), 67–72.

[51] Sture, S., Runesson, K., and Macari-Pasqualino, E. J. Analysis and calibration of a three invariant plasticity model for granular materials. *Ingenieur Archiv 59* (1989), 253–266.

[52] Szabó, L., and Balla, M. Comparison of some stress rates. *International Journal of Solids and Structures 25*, 3 (1989), 279–297.

[53] Ting, T. C. T. Determination of $C^{1/2}$, $C^{-1/2}$ and more general isotropic tensor functions of C. *Journal of Elasticity 15* (1985), 319–323.